Research Square

Preprints are preliminary reports that have not undergone peer review.
They should not be considered conclusive, used to inform clinical practice,
or referenced by the media as validated information.

Non-canonical mutations drive the evolution of persistent Staphylococcus aureus small-colony variants under zinc oxide nanoparticle stress

Anjali Jaiswal
University of Delhi South Campus
Sambuddha Chakraborty
University of Delhi South Campus
Akshit Malhotra
University of Delhi South Campus
Sangita Jana
University of Delhi South Campus
Ram Karan
University of Delhi South Campus
Ashwini Chauhan
ashwinichauhan@south.du.ac.in

University of Delhi South Campus

Article

Keywords:

Posted Date: October 20th, 2026

DOI: https://doi.org/10.21203/rs.3.rs-11136755/v1

License: This work is licensed under a Creative Commons Attribution 4.0 International License.
Read Full License

Additional Declarations: No competing interests reported.

Non-canonical mutations drive the evolution of persistent *Staphylococcus aureus* small-colony variants under zinc oxide nanoparticle stress

Anjali Jaiswal[1], Sambuddha Chakraborty[1], Akshit Malhotra[1], Sangita Jana[1], Ram Karan[1], Ashwini Chauhan[1]*

[1] Department of Microbiology, University of Delhi South Campus, Benito Jaurez Marg, New Delhi 110021, India

* Correspondence: ashwinichauhan@south.du.ac.in

Abstract

The widespread application of Zinc Oxide Nanoparticles (ZnO NPs) in industrial and medical products necessitates a rigorous understanding of bacterial adaptive trajectories under sustained exposure to nanomaterials. In this study, we employed experimental evolution, quantitative proteomics and whole-genome sequencing to investigate the long-term response of *Staphylococcus aureus* to subinhibitory concentrations of ZnO NPs. Serial passaging in the presence of 500 µg/ml ZnO NPs for 14 passages progressively enriched Small Colony Variants (SCVs), which exceeded 95% of the population by passage 10 and became dominant by passage 12; the phenotype remained stable after removal of ZnO NPs. Compared with the parental strain, the evolved SCV exhibited approximately fourfold increase in generation time, increased cell diameter (535 versus 390 nm) and cell-wall thickness (44 versus 29 nm), reduced susceptibility to ZnO NPs with about 68% killing compared to 99.9% killing, and increased adherence to A549 cells (75.45 versus 54.72%). Whole-genome sequencing identified nonsynonymous mutations in *mprF*, *rpsE*, *gyrA*, *comEB*, and *yqeH*, and revealed loss of an approximately 19 kb plasmid carrying *blaZ* and its regulatory genes. Remarkably, despite loss of this plasmid, β-lactam resistance increased markedly, with penicillin G and ampicillin MICs increasing from 32 to 512 µg/ml and from 64 to 1024 µg/ml, respectively. These findings show that continuous ZnO NP

exposure can select for a stable SCV phenotype accompanied by metabolic and structural remodelling and altered antibiotic susceptibility, highlighting an evolutionary consideration for the prolonged use of ZnO NP based antimicrobial materials.

Introduction

The rapid global emergence of antimicrobial resistance (AMR) is dismantling the efficacy of antibiotic pharmacopoeia, pushing clinical medicine towards a precarious post-antibiotic era, a critical challenge to public health. This situation has created an urgent need for innovative alternative interventions.[1,2] Among these alternatives, metal-based nanoparticles have emerged at the forefront of nanomedicine, as they offer a poly-pharmacological approach due to their effective broad-spectrum antimicrobial activity and multi-modal mechanisms of action[3]. In particular, zinc oxide nanoparticles (ZnO NPs) are widely deployed in advanced biomedical applications, such as wound dressings[4], medical device coatings[5], and disinfectant surfaces.[6] This multifaceted antimicrobial profile is largely attributed to their reliance on reactive oxygen species (ROS) mediated oxidative damage and Zn^{2+} induced membrane damage[3]. This has fostered the prevailing view that ZnO NPs exert a non-specific physical pressure that is inherently resistant to classical bacterial evasion strategies. As of 2012, the global annual production of ZnO NPs was estimated at approximately 550 metric tons, contributing to a cumulative production of 58,000 metric tons of engineered nanomaterials annually by 2020.[7] The escalating environmental and clinical footprint of metal oxide nanoparticles has established a chronic selective landscape, raising urgent concerns regarding the potential for microbial adaptation and the emergence of persistent reservoirs.[8] Current paradigms of nanotoxicity resistance are largely centered on silver nanoparticles, where evasion is mediated by physical exclusion, flagellar motility, and biochemical detoxification through efflux pumps.[9,10] Furthermore, *Acinetobacter baumannii* has been shown to acquire silver nanoparticle (AgNP) resistance through specific genotypic alterations in cell attachment and capsular polysaccharide biosynthesis.[11] These mutations catalyze a systemic

physiological restructuring, enabling the pathogen to quench oxidative stress and reconfigure its metabolic flux to survive chronic AgNP exposure. While evidence of bacterial adaptation to silver nanoparticles continues to surface, a major knowledge gap persists regarding the evolutionary risks associated with Zinc Oxide NPs. Addressing this is vital, as the widespread dissemination of ZnO NPs may inadvertently select for persistent microbial variants uniquely adapted to withstand multifaceted inorganic stress.

Recent experimental evolution studies suggest that *E. coli* developed adaptive resistance to ZnO NPs upon prolonged exposure, accompanied by morphological changes and differential expression of membrane- associated proteins.[12] However, a fundamental question remains: can ZnO NP stress drive permanent, heritable adaptations in high-priority clinical pathogens? To date, a stable or genetically encoded resistance mechanism to ZnO NPs has remained elusive.

Unlike the gen-centric nature of classical antibiotic resistance, nanoparticle adaptation is considered as a complex, multifactorial process involving metabolic rewiring and phenotypic heterogeneity.[13] One such adaptive phenotype is the small colony variant (SCV), a slow-growing, metabolically altered subpopulation characterized with intracellular persistence, stress tolerance, and antimicrobial evasion.[14,15] Although SCVs have been extensively studied in the context of chronic infections and antibiotic exposure, their emergence in response to nanoparticle stress and whether their transition is genetically anchored remain critical new frontiers in understanding microbial persistence.

In this study, we combined quantitative proteomics, experimental evolution, and whole-genome sequencing (WGS) to explore how *S. aureus* adapts to sustained exposure to sub-inhibitory concentrations of ZnO nanoparticles. We aimed to determine whether continuous exposure to ZnO NPs could select for a stable, heritable SCV phenotype and whether this adaptation was accompanied by changes in susceptibility to conventional antibiotics. By defining the phenotypic and genetic features associated with prolonged ZnO NP exposure, this study addresses the

potential for nanoparticle-mediated selection to influence bacterial persistence and antibiotic resistance.

These findings redefine our understanding of nanoparticle-microbe interactions and provide the first evidence of a genetically anchored ZnO nanoparticle-driven adaptation, uncovering a previously unrecognized mechanism towards chronic infection.

Results and Discussion

ZnO nanoparticles exhibit dose-dependent killing of *S. aureus* while leaving a resilient subpopulation

To evaluate the antibacterial efficacy of the synthesized ZnO NPs, we conducted *in- vitro* killing assay against *S. aureus* SAW 1 **(Figure 1A)**. Exposure to ZnO NPs for 24 h exhibited a concentration-dependent reduction in bacterial survival, achieving about a 3 $\log_{10}$ reduction at 250, 500, and 750 µg/ml. This pattern is consistent with published reports on ZnO nanostructures, where concentration-dependent antibacterial activity of ZnO nanoparticles has been well documented against *S. aureus* using colony-forming unit enumeration after 24 h of incubation.[16,17]

Notably, ZnO nanoparticles have been reported to decrease the number of CFU/ml by 3 $\log_{10}$ units against *S. aureus* strains[18] corroborating our findings. Despite this potent activity, complete sterilization was not attained at any concentration tested, as a small proportion of cells remained viable across all conditions **(Figure 1B)**. This is consistent with the well-established phenomenon of bacterial persistence, wherein a small fraction of the bacterial population survives lethal antimicrobial exposure while remaining genetically susceptible, and can resume growth once the stressor is removed.[19] Such surviving subpopulations have been observed not only with conventional antibiotics but also with nanomaterial-based antimicrobials, and spontaneous persistence leads to a constant fraction of surviving cells in a population (usually between 0.001% and 1%), ensuring bacterial survival under stress conditions.[20]

To confirm that this antibacterial efficacy was supported by colloidal stability throughout the 24 h assay, the physical state of the ZnO NPs was evaluated in TSB media. UV-Vis absorption spectra exhibited a distinct surface excitation peak at 370 nm that remained unchanged after 24 h of incubation at 37°C, showing no peak shift or broadening **(Figure S1A).** This distinct 370 nm band is a well-established spectroscopic hallmark of nanoscale zinc oxide, arising from intrinsic electron transitions from the valence band to the conduction band ($O_{2p} \rightarrow Zn_{3d}$) under quantum confinement conditions. The preserved peak symmetry and spectral stability confirm that interaction with TSB nutrients such as peptones and amino acids-likely formed a protective organic media corona that hindered kinetic agglomeration rather than triggering rapid micro-scale precipitation.[21,22]

Nanoparticle Tracking Analysis (NTA) confirmed uniform dispersion, revealing a modal hydrodynamic diameter of 92.3 ± 3.1 nm of 89.9 nm merged mode and a mean hydrodynamic diameter of 127.9 ±1.0 nm of D_{10} = 82.8 nm, D_{50} = 111.4 nm, D_{90} = 196.2 nm **(Figure S1B-C and Table S1),** with real-time video tracking confirming individual particles undergoing Brownian diffusion without micro-scale cluster formation.

To investigate the mechanism underlying this bactericidal activity, intracellular ROS levels were quantified using the DCFDA fluorescence assay. 2′,7′-Dichlorodihydrofluorescein diacetate (DCFH-DA) is one of the most widely used techniques for directly measuring the redox state of a cell[23], and has been validated for use in bacterial systems exposed to metal oxide nanoparticles. Cells exposed to ZnO nanoparticles exhibited a marked elevation in intracellular ROS compared to untreated controls **(Figure 1C)**. Elevated intracellular ROS generation in *S. aureus* cells incubated with ZnO nanoparticles compared to non-treated controls is strongly related to their antimicrobial activity.[24] These findings implicate oxidative stress as a key contributor to the antibacterial action of ZnO nanoparticles, in agreement with the widely supported mechanistic model in which oxidative stress induced by excess ROS plays a substantial role in inducing lipid peroxidation on the bacterial cell membrane, ultimately contributing to cell death.[25,26]

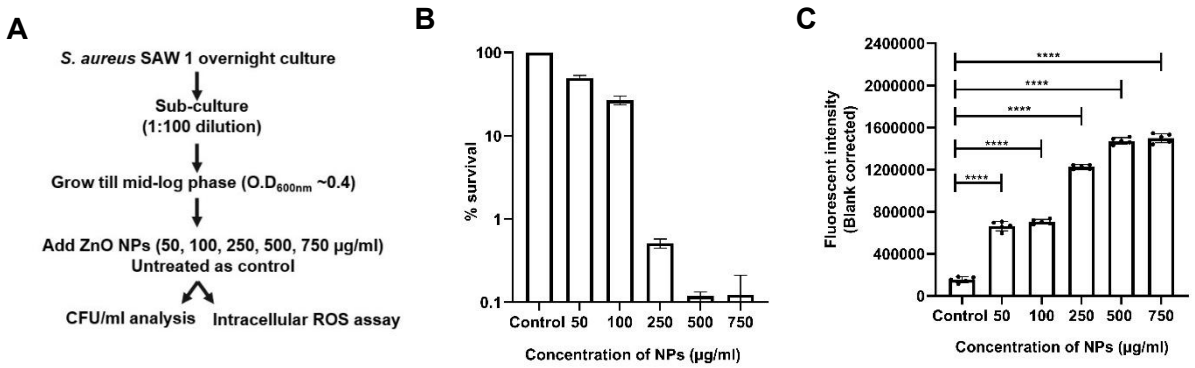


Figure 1. Zinc oxide nanoparticles (ZnO NPs) exhibit concentration dependent antibacterial activity and induce ROS. (A) Schematic representation of experimental design. (B) Percent survival of *S. aureus* SAW1 following 24 h exposure to increasing concentrations of ZnO nanoparticles (50 to 750 µg/ml). A concentration-dependent reduction in bacterial survival was observed, with about a 3 $\log_{10}$ reduction at concentrations 500 and 750 µg/ml. Despite substantial killing, a small surviving subpopulation remained detectable even at high concentration of ZnO nanoparticles. (C) Intracellular reactive oxygen species (ROS) levels measured by the DCFH-DA fluorescence assay following ZnO NP exposure. ZnO NP treatment induced a concentration-dependent increase in ROS production relative to untreated controls, indicating enhanced oxidative stress. Each condition was tested in five replicates (n = 5). Statistical analysis in (C) was performed using one-way ANOVA followed by Dunnett's multiple-comparisons test, comparing each ZnO NP-treated group with the untreated control. All comparisons were statistically significant (****adjusted $p < 0.0001$).

ZnO nanoparticle stress induces proteomic reprogramming associated with SCV emergence

Despite the potent antibacterial activity and ROS induction mediated by ZnO NPs, a small fraction of *S. aureus* cells remained viable following treatment. To gain a comprehensive understanding of the global cellular response of this surviving subpopulation under ZnO NP-induced stress, we performed comparative proteomic analysis. This approach enabled the

identification of differentially expressed proteins and pathways associated with the bacterial response to nanoparticle exposure at the protein level.

We analyzed the proteomic profile of *S. aureus* following ZnO NPs treatment (500 µg/ml) to characterize the protein-level changes in the bacterial population recovered after nanoparticle treatment **(Figure 2A)**. We identified 763 proteins with differential expression following treatment, of which 246 were significantly differentially expressed ($P \leq 0.05$, $\log_2$ fold change ≥ 0.5). Among these, 138 proteins were downregulated, while 108 exhibited upregulated expression **(Figure 2B-a)**.

The most prominently down-regulated protein was the large-conductance mechanosensitive channel (MscL), a key bacterial membrane valve that safeguards cells from osmotic imbalance and membrane tension by regulating cytoplasmic volume under external stress conditions[27]. It's down-regulation under ZnO NP stress likely reflects a compromise in the cell's capacity to manage membrane tension and osmotic challenges. Conversely, Conserved Virulence Factor B (CvfB), an RNA-binding protein involved in virulence regulation, stress response, and metabolism-displayed the greatest up-regulation **(Figure 2B-b)**. Previous studies have shown that the CvfB contains multiple RNA-binding domains and functions as a post-transcriptional regulator that modulates the expression of genes involved in bacterial physiology and pathogenicity[28]. Functional enrichment analysis (*score* > 1.5) of significantly down-regulated proteins underscored broad suppression of bacterial metabolism, most prominently glycolysis/ gluconeogenesis (cluster of 13 proteins) and amino acid metabolism (cluster of 11 proteins) **(Figure 2C, Table S2; Figure S2A)**

Additionally, proteins involved in chaperone-mediated folding and unfolded protein binding were significantly diminished, indicative of an attenuated canonical stress response, suggesting a shift towards metabolic dormancy. In contrast, proteins linked to ribosomal biogenesis and translation were markedly up-regulated, suggesting a selective enhancement of translational capacity

(Figure 2B c-d). Furthermore, gene ontology analysis revealed cellular components experienced the most substantial remodeling of cellular components, with 86 affected proteins differentially expressed; notably, half of them were up-regulated, and the remaining 43 were down-regulated, highlighting the struggle of the ZnO NP-treated cells to maintain homeostasis **(Figure S2 B-C)**.

To further explore functional connectivity among deregulated proteins, STRING protein–protein interaction (PPI) analysis was performed. The analysis revealed distinct interaction modules corresponding to translation, central metabolism, cell wall modulation, stress response, and DNA repair pathways, highlighting coordinated pathway-level remodelling rather than isolated protein changes **(Figure S3)**. The up-regulated protein network was particularly abundant in ribosomal proteins, cell-envelope/cell-shape-associated proteins, and factors involved in DNA repair. The dense network among ribosomal proteins may indicate that the translational machinery is undergoing coordinated remodeling as a response to stress induced by nanoparticles. Similar alterations in ribosome-associated proteins have been reported during bacterial adaptation to environmental stress. Proteomic analyses of *S. aureus* under osmotic stress have also identified structural ribosomal proteins among the major differentially abundant proteins.[29] The PcrA-centered interaction network further highlighted the involvement of genome maintenance processes in the response to ZnO NP exposure. PcrA is a DNA helicase involved in DNA replication, recombination, and repair, and its increased abundance within the interaction network may reflect an elevated requirement for genome maintenance under nanoparticle-induced stress. This observation is consistent with previous evidence that ZnO NPs can induce oxidative stress and DNA damage, while studies in *S. aureus* have linked zinc homeostasis to the maintenance of genome integrity and DNA damage repair. Thus, the enrichment of DNA repair-associated interactions, together with the ROS response observed in our study, suggests that ZnO NP exposure imposes oxidative and metal-associated stress that may increase the cellular demand for genome maintenance.[30,31]

The MreA/MreB associated cluster further suggests that ZnO NP exposure affects cell-envelope and cell-shape homeostasis. This is consistent with previous studies showing that ZnO NPs compromise bacterial membrane integrity and induce morphological damage, including membrane disruption and intracellular leakage. Such envelope perturbation may increase the requirement for coordinated regulation of proteins involved in maintaining cell architecture and membrane-associated processes.[32,33]

In contrast, the down-regulated networks were dominated by interconnected metabolic modules, including heme biosynthesis, purine metabolism, sulfur/amino-acid metabolism, and stress/proteostasis functions. The suppression of these metabolically connected pathways suggests a broader reduction or reprogramming of anabolic and energy-demanding processes following ZnO NP exposure. This observation is consistent with previous proteomic studies showing that ZnO exposure can cause widespread metabolic reorientation, including perturbation of amino-acid, nucleotide, energy, and sulfur metabolism. In *Bacillus subtilis*, ZnO-induced proteomic remodeling was associated with altered central and sulfur-amino-acid metabolism and activation of the stringent stress response, whereas studies in *Salmonella* have reported broad suppression of translation, amino-acid biosynthesis, nucleotide metabolism, and energy-generating pathways following ZnO exposure. [34, 35] More recently, integrated analyses of metal stress in *S. aureus* have similarly demonstrated disruption of central carbon metabolism, respiration, ATP production, and cell-wall biosynthesis, emphasizing the close relationship between metal dysregulation, metabolic collapse, and envelope stress.[36]

Following treatment of planktonic *S. aureus* cells with ZnO NPs, we observed the emergence of a phenotypically distinct small colony variant (SCV) at a mean frequency of 4.45 ± 1.05% (n = 3) upon extended incubation of the plates. SCV frequency was determined by examining 100 colonies per replicate and recording the proportion that exhibited SCV morphology; no SCVs were detected in the untreated control population under identical plating conditions.

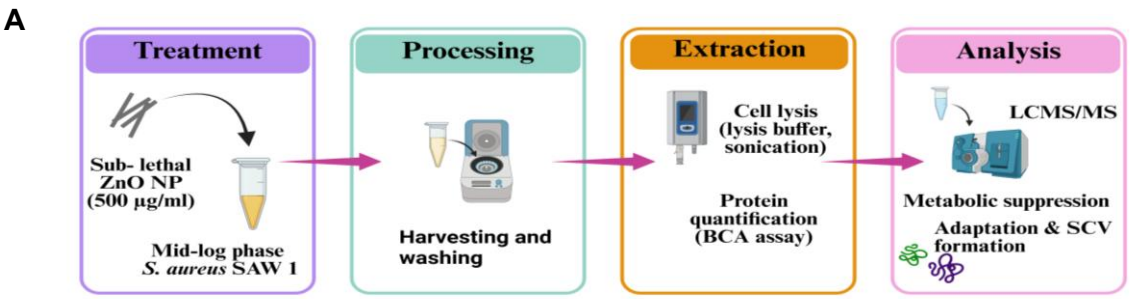
S. aureus SCVs are linked to chronic, recurrent, and antibiotic-resistant infections, and an important part of their ability to persist is associated with a quiescent metabolic state.[37] Interestingly, the proteomic profile of ZnO NPs-treated cells was concordant with the emergence of small colony variants- a reported phenotypic variant of *S. aureus* under antimicrobial treatment- indicating their critical role in protein-level adaptations in post-treatment bacterial survival. The key proteins up-regulated in this context included Obg (a GTPase associated with persistence under nutrient stress and functions by affecting the ribosome assembly)[38] MazF (a toxin-antitoxin system component linked to dormancy and involved affecting translation directly by cleaving mRNAs)[39], and MgrA (a global regulator modulating virulence and antibiotic resistance).[40] Concurrently, enzymes central to menaquinone biosynthesis (MenA), heme biosynthesis (HemB), central metabolism (PdhA), and peptidoglycan synthesis (MurA) were significantly elevated **(Figure 2B; Table S3A; S3B)**, supporting a metabolic reprogramming characteristic of the SCV physiology.

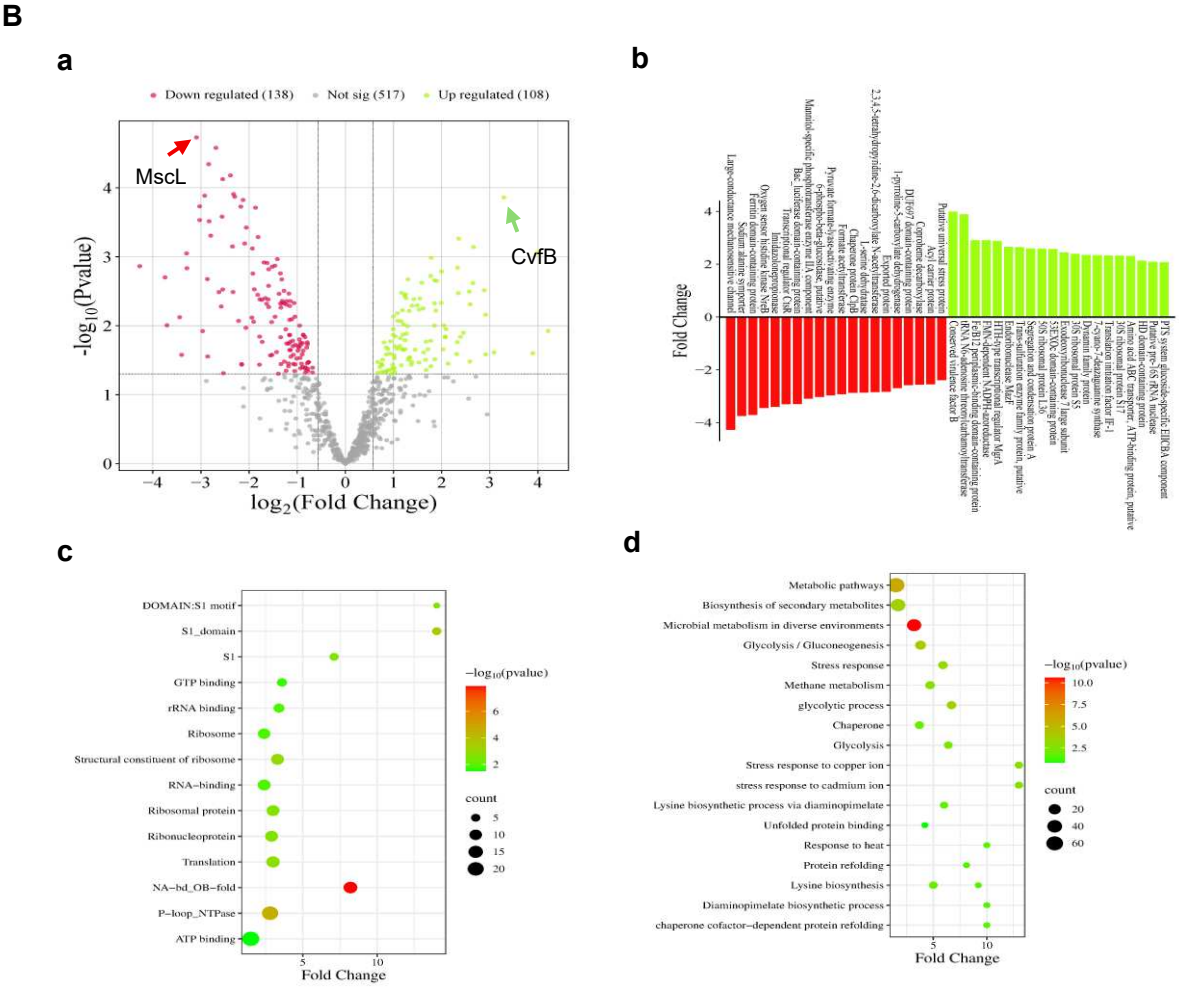
The proteomic landscape also revealed broad suppression of adaptive pathways central to bacterial survival under stress. Notably, a ferritin domain- containing protein was strongly down-regulated (3.71-fold), implicating disrupted iron storage and detoxification; bacterial ferritins buffer excess metal ions to mitigate Fenton chemistry-driven oxidative damage, and their depletion may exacerbate nanoparticle-induced ROS stress.[41] The sodium: alanine symporter showed a 3.75-fold reduction, reflecting inhibited amino acid uptake and osmoregulatory transport. Prokaryotic Na^+/solute symporters are pivotal for nutrient acquisition and osmotic balance, and their suppression aligns with the metabolic slowdown characteristic of SCVs.[42]

Additionally, the oxygen sensor histidine kinase NreB was down-regulated by 3.44-fold, suggesting weakened environmental sensing and redox signaling capacity; two-component histidine kinases like NreB modulate gene expression in response to oxygen fluctuations, and their inhibition may blunt aerobic respiration adjustments under oxidative stress.[43] Down-

regulation of stress response regulators driving emergence of SCV also corroborates with previous study.[15] Up-regulation of ABC transporter substrate-binding proteins (2.30-fold) further points to restricted nutrient and metal ion uptake, while the decrease in the serine protease HtrA-like protein (2.55-fold) indicates impaired periplasmic protein quality control and stress-induced proteostasis.[44]

The proteomic signatures also included reduced expression of key glycolytic enzymes such as Pgk, Ldh1, and GpmA, as well as TCA cycle enzymes including FumC and Mqo **(Figure 2B)** This metabolic down-shift aligns with a low-energy state commonly associated with stable SCVs. Universal to all SCV phenotypes, including clinical isolates and site-directed mutants is a characteristic reduction in central metabolic carbon flux and citric acid cycle activity, independent of the specific auxotrophic driver.[45, 46] Collectively, the proteomic data revealed that ZnO NP-treated *S. aureus* initiates a coordinated stress adaptation program by increased translation, suppressed metabolic activity, and induction of SCV-associated determinants, facilitating the emergence of a metabolically rewired and persistence-capable SCV population.


A
Treatment
Sub- lethal ZnO NP (500 µg/ml)
Mid-log phase S. aureus SAW 1
Processing
Harvesting and washing
Extraction
Cell lysis (lysis buffer, sonication)
Protein quantification (BCA assay)
Analysis
LCMS/MS
Metabolic suppression
Adaptation & SCV formation


B
a
Down regulated (138)
Not sig (517)
Up regulated (108)
MscL
CvfB
-log10(Pvalue)
log2(Fold Change)
b
Fold Change
c
DOMAIN:S1 motif
S1_domain
S1
GTP binding
rRNA binding
Ribosome
Structural constituent of ribosome
RNA-binding
Ribosomal protein
Ribonucleoprotein
Translation
NA-bd_OB-fold
P-loop_NTPase
ATP binding
−log10(pvalue)
count
Fold Change
d
Metabolic pathways
Biosynthesis of secondary metabolites
Microbial metabolism in diverse environments
Glycolysis / Gluconeogenesis
Stress response
Methane metabolism
glycolytic process
Chaperone
Glycolysis
Stress response to copper ion
stress response to cadmium ion
Lysine biosynthetic process via diaminopimelate
Unfolded protein binding
Response to heat
Protein refolding
Lysine biosynthesis
Diaminopimelate biosynthetic process
chaperone cofactor−dependent protein refolding
−log10(pvalue)
count
Fold Change

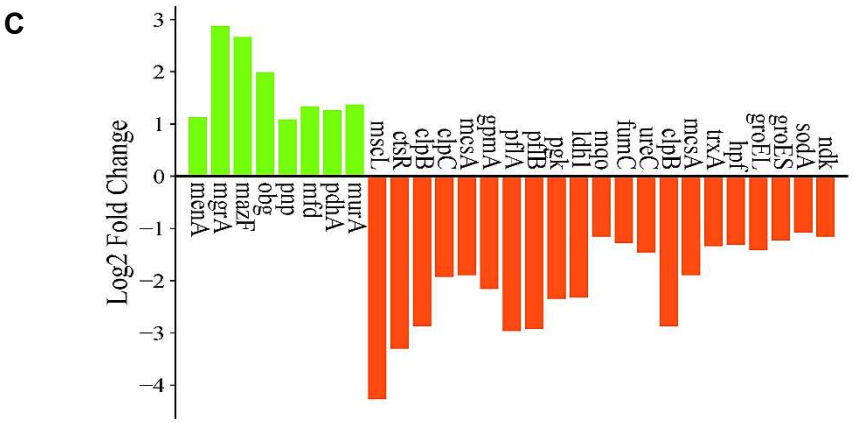

C
Log2 Fold Change
menA
mgrA
mazF
obg
pnp
mfd
pdhA
murA
mscL
ctsR
clpB
clpC
mcsA
gpmA
pfkA
pfkB
pgk
ldh1
mqo
fumC
ureC
clpB
mcsA
trxA
hpf
groEL
groES
sodA
ndk

Figure 2. Proteomic response of *S. aureus* to ZnO nanoparticle exposure. (A) Schematic representation of the experimental workflow for proteomic analysis of ZnO NP-treated *S. aureus*. (B) Overview of the proteomic changes following ZnO NP treatment. (a) Volcano plot showing significantly differentially expressed proteins, with significantly up-regulated proteins shown in green and down-regulated proteins shown in red. The positions of selected proteins discussed in the text, including MscL and CvfB, are indicated. (b) Top 20 up-regulated and down-regulated proteins identified following ZnO NP exposure. (c, d) Enrichment analysis of significantly up-regulated and down-regulated proteins, respectively. Dot size represents the number of proteins associated with each enriched term, and colour represents the degree of enrichment (fold enrichment). (C) Differentially abundant proteins associated with the SCV phenotype following ZnO nanoparticle exposure. The bar graph shows the $\log_2$ fold change in abundance of selected proteins in ZnO NP-treated cells relative to the untreated wild-type strain. Up-regulated proteins are shown in green and down-regulated proteins in red. Selected proteins include MenA, MurA and ObgF among the up-regulated proteins, and ClpC, GroEL, TrxA and SodA among the down-regulated proteins.

ZnO exposure induces emergence of slow-growing, de-pigmented SCVs in *S. aureus*

Interestingly, the proteomic analysis revealed the differential expression of several proteins previously associated with stress adaptation, metabolic reprogramming, and small colony variant (SCV)-like phenotype in *S. aureus*. Since routine post-treatment plating had initially been performed using standard overnight incubation (16-18 h), such slow-growing phenotypic variants may have remained undetected. Therefore, to further investigate whether ZnO NP exposure induced observable phenotypic heterogeneity, we extended the incubation period of treated cultures and carefully monitored colony morphology over time for the emergence of slow-growing variants.

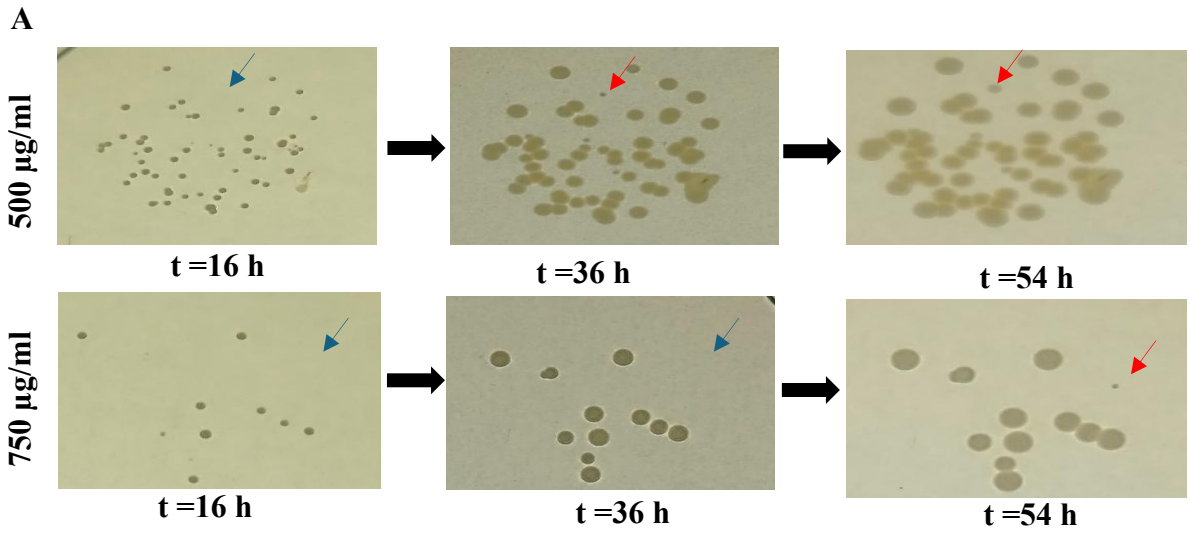
To investigate the phenotypic consequences of ZnO NP treatment, we exposed *S. aureus* SAW1 to 500 and 750 µg/ml ZnO NPs for 24 h, with colony morphology monitored over extended incubation. Distinct SCVs emerged, characterized by markedly reduced colony size, loss of pigmentation, and delayed growth compared to the WT population.

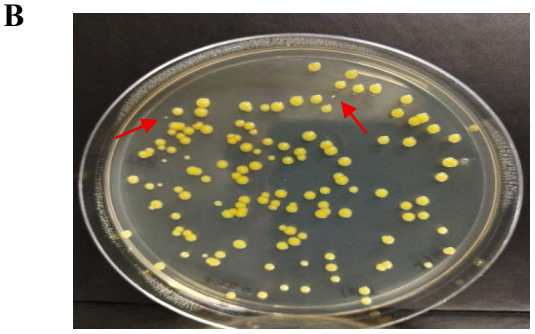
These SCVs were detectable by 36 h and became prominent by 54 h following exposure to 500 and 750 µg/mL ZnO NPs **(Figure 3A).** Representative 48 h images confirmed a heterogeneous population structure, with depigmented small colonies that were approximately 1/10th the size of normal WT colonies. **(Figure 3B-C).** The emergence of depigmented, slow-growing SCVs following ZnO NP treatment is consistent with previous reports describing oxidative stress-mediated adaptive responses in *S. aureus*.[46] ROS generated during ZnO NP exposure can disrupt the electron transport chain, cellular respiration, and membrane homeostasis, thereby promoting the formation of metabolically altered SCVs. Importantly, staphyloxanthin pigmentation in *S. aureus* is closely linked to oxidative stress defense; therefore, the observed loss of pigmentation in ZnO NP derived SCVs likely reflects disruption of redox homeostasis and metabolic remodeling under nanoparticle-induced stress conditions.[47]

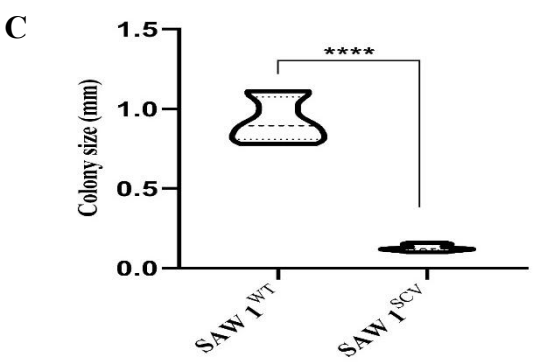
Transmission electron microscopy (TEM) revealed pronounced morphological differences between SCV and WT cells **(Figures 3D-E).** SCVs exhibited a significantly larger average cell diameter (~535 nm) compared to WT cells (~390 nm; $p < 0.0001$), alongside substantial cell wall thickening (~44 nm vs. ~29 nm; $p < 0.0001$) **(Figures 3F-G)**. This represents 51.72 % increase in cell-wall thickness and may contribute to the altered susceptibility of SCVs to β-lactam antibiotics by affecting cell-envelope structure and antibiotic access to their targets.

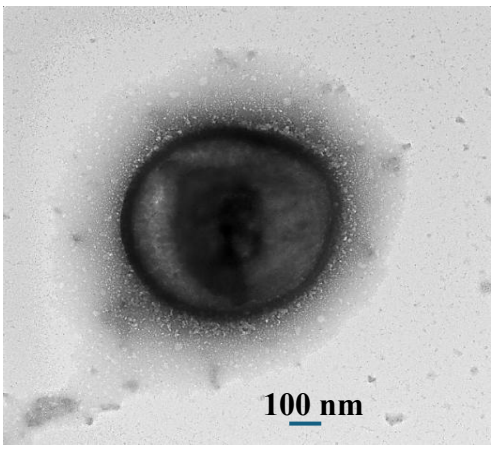
High-resolution TEM further documented abnormal septation and cell aggregation, hallmarks of a stress adapted phenotype. Similar observations have been reported in the study showing SCVs associated with the chronic prosthetic infections displayed significantly increased cell wall thickness compared to the wildtype counterparts.[15] Furthermore, studies have shown that oxidative stress acts as a powerful environmental cue that triggers profound structural and metabolic remodelling. When bacteria encounter ROS or subinhibitory antimicrobial pressure, they redirect energy away from rapid replication and into survival mechanisms. This stress response often down-regulates standard cell division machineries while altering cell wall

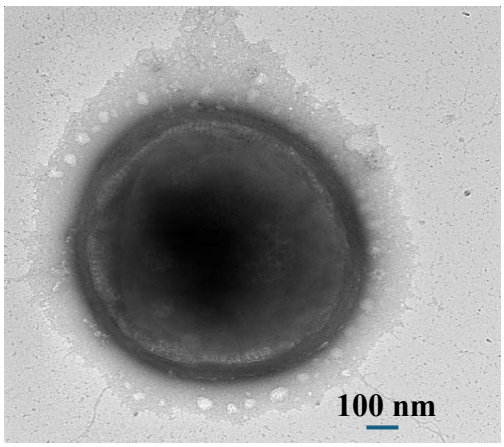
biosynthetic pathways.[48] The accumulation of oxidative damage and subsequent metabolic rewiring force the cells into an abnormal cell size, resulting in distinct morphological variations-such as cell elongation (filamentation) or swelling-and the population-level appearance of slow-growing, highly resilient small-colony variants.[49, 50] Together, these results demonstrate that the subinhibitory exposure to ZnO NPs drives the emergence of *S. aureus* SCVs characterized by altered colony morphology, and ultrastructural remodelling. This phenotypic switch likely represents an adaptive survival strategy under nanoparticle-induced stress conditions.

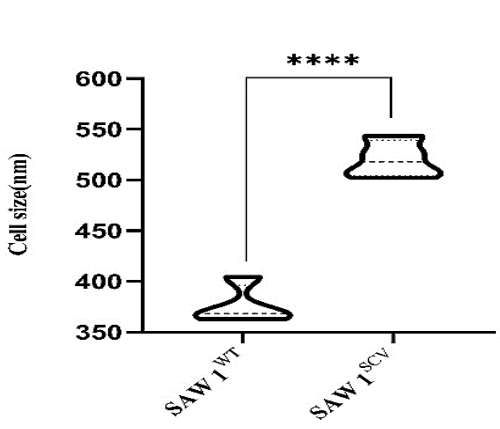

A
500 µg/ml
t =16 h
t =36 h
t =54 h
750 µg/ml
t =16 h
t =36 h
t =54 h


B


C
Colony size (mm)
1.5
1.0
0.5
0.0
****
SAW 1 WT
SAW 1 SCV


D
100 nm


E
100 nm


F
Cell size(nm)
600
550
500
450
400
350
****
SAW 1 WT
SAW 1 SCV

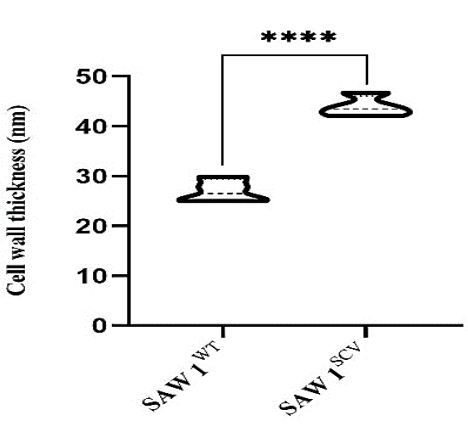

G
Cell wall thickness (nm)
50
40
30
20
10
0
****
SAW 1 WT
SAW 1 SCV

Figure 3: Emergence and characterization of small colony variants (SCVs) in *S. aureus* upon prolonged exposure to ZnO NPs. A: Representative images show colony morphology on TSA plates at 500 µg/ml and 750 µg/ml ZnO NP concentrations over three time points: 16 h, 36 h, and 54 h post-incubation. Red arrows indicate the small colonies that emerged during extended incubation, whereas blue arrows indicate regions where SCVs were not observed at the corresponding time point. **B:** Representative image of altered pigmentation of SCV compared to normal WT colony. **C:** Violin plot showing the distribution of colony sizes for WT and SCV. SCVs exhibited a significantly smaller colony diameter compared to the WT strain (****$p < 0.0001$). **D:** Transmission Electron Microscopy (TEM) micrograph of *S. aureus* WT colony showing typical coccoid morphology with uniform cell size. **E:** TEM micrograph of SCV colony displaying increased cell size and thickened cell walls. **F-G**: TEM analysis of cell morphology in WT and small colony variant (SCV). **F:** Violin plot representing a significant increase in mean cell size of SCV isolates compared to WT cells, as determined by TEM (****$p < 0.0001$; $n = 5$). **G:** Violin plot showing a statistically significant increase in cell wall thickness in SCV isolates relative to the WT strain (****$p < 0.0001$; $n = 5$). For panels F and G, measurements were obtained from 5 cells per group from a single TEM preparation. Data are presented as mean ± SD, and statistical significance was determined using an unpaired two-tailed Student's t-test. The scale bar represents 100 nm in the micrograph.

Repeated ZnO nanoparticle exposure selects for a stable SCV phenotype

As SCVs recovered following ZnO nanoparticle exposure reverted to the normal-sized wildtype upon sub-culturing them into nanoparticle free LB media, a phenomenon widely reported for unstable, transient SCVs.[46, 50] To determine whether sustained nanoparticle exposure could drive phenotypic stabilization and selection of a persistently adapted subpopulation, transient SCVs were subjected to prolonged serial passaging (P1-P14) in media supplemented with 500 µg/ml ZnO NPs **(Figure 4A)**. The SCV population progressively enriched with each passage, exceeding 95% by passage 10 and becoming completely dominant by passage 12. By passage 14 (P14), the SCV phenotype exhibited irreversible morphological stability, with no reversion to the WT colony type even after multiple subcultures in NP-free conditions **(Figures 4B-C)**.

Colonies consistently exhibited reduced size and hypopigmentation across passages, indicating phenotypic stabilization. Similar stabilization has been documented during serial passaging with increasing concentrations of THAM-3ΦG[50] or aminoglycosides, where SCVs

displayed increased MICs and prolonged generation times, consistent with slow- growing SCV phenotype.[51]

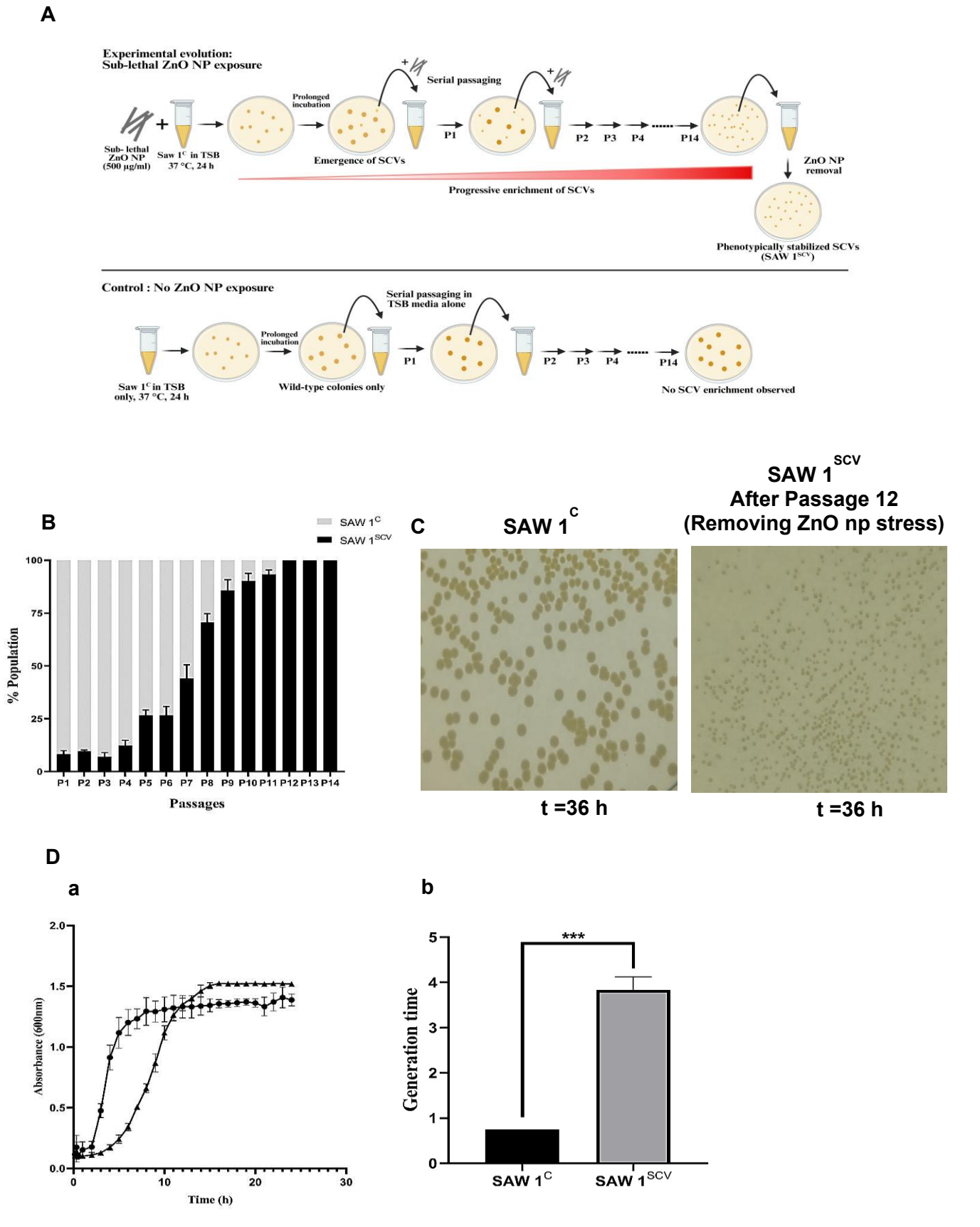
The physiological characterization of stabilized SCVs revealed pronounced growth alterations. The growth profiling in TSB showed SCVs demonstrated a prolonged lag phase and a reduced exponential growth rate, with approximately fourfold increase in generation time compared to WT cells ($p < 0.0001$) **(Figure 4D-E)**.

Earlier studies have shown that *S. aureus* SCVs exhibit resistance to aminoglycosides due to impaired electron transport chains, reducing antibiotic uptake and enhancing persistence.[42] Moreover, SCVs alter antibiotic susceptibility profiles variably, with resistance to antibiotics like erythromycin and kanamycin, alongside continued susceptibility to others such as ampicillin and polymyxin-particularly observed in *E. coli.*[52] In our study, antimicrobial susceptibility testing using Kirby-Bauer disc diffusion assays on 22 antibiotics revealed that SCVs exhibited altered susceptibility particularly against β-lactams (ampicillin, ceftazidime, penicillin) and ciprofloxacin **(Table S4A)**. Minimum inhibitory concentration (MIC) assays of selected antibiotics confirmed increased resistance to β-lactam antibiotics targeting penicillin-binding proteins (PBPs), with MICs of penicillin G and ampicillin increasing from 32 to 512 µg/ml and from 64 to 1024 µg/ml, respectively, in $SAW1^{SCV}$ compared with the parental $SAW1^{C}$ strain **(Table S 4B).**

These findings suggest that the adaptive changes associated with ZnO NP-enriched SCV formation can confer altered antibiotic susceptibility and may instead involve physiological trade-offs that enhance survival under nanoparticle stress and certain antimicrobial agents. Nevertheless, ZnO nanoparticles killing assays demonstrated reduced bactericidal efficacy against SCVs (~68% killing) relative to WT cells (99.9% killing). Nevertheless, ZnO nanoparticles killing assays demonstrated reduced bactericidal efficacy against SCVs (~68% killing) relative to WT cells (99.9% killing). Furthermore, evolved SCVs showed significant increase in the biofilm formation as determined by viable-cell enumeration of biofilms ($p<0.05$). **(Figure S4)**.

Clinically, SCVs pose significant challenges due to their persistence in host tissues and evasion of immune clearance.[36,53] We have found that SCVs adhered more efficiently to A549 epithelial cells and showing 1.38-fold greater adherence ($p < 0.01$) and persisted intracellularly in THP-1 macrophages. In THP-1 macrophages, intracellular survival was comparable between $SAW1^{C}$ and $SAW1^{SCV}$ at 15 min, followed by a transient decrease at 6 h and subsequent recovery at 12 and 24 h. At 24 h, $SAW1^{SCV}$ showed approximately 58% intracellular survival compared with approximately 31% for $SAW1^{C}$ **(Figure 4F-G)**. This mirrors previous findings showing SCVs evade host immune responses, promoting chronic and relapsing infections.[36,54]

Together, these results establish that sustained ZnO NP exposure selects for a phenotypically stable SCV subpopulation characterized by slow growth, altered susceptibility to antibiotics and nanoparticles, improved host cell interaction and intracellular persistence, hallmarks of a chronic, stress-adapted bacterial phenotype.


A
Experimental evolution:
Sub-lethal ZnO NP exposure
Sub- lethal ZnO NP (500 µg/ml)
Saw 1C in TSB 37 °C, 24 h
Prolonged incubation
Emergence of SCVs
Serial passaging
P1
P2
P3
P4
P14
Progressive enrichment of SCVs
ZnO NP removal
Phenotypically stabilized SCVs (SAW 1SCV)
Control : No ZnO NP exposure
Saw 1C in TSB only, 37 °C, 24 h
Prolonged incubation
Wild-type colonies only
Serial passaging in TSB media alone
No SCV enrichment observed
B
SAW 1C
SAW 1SCV
% Population
Passages
C
SAW 1C
SAW 1SCV After Passage 12 (Removing ZnO np stress)
t =36 h
t =36 h
D
a
Absorbance (600nm)
Time (h)
b
Generation time
***
SAW 1C
SAW 1SCV

426

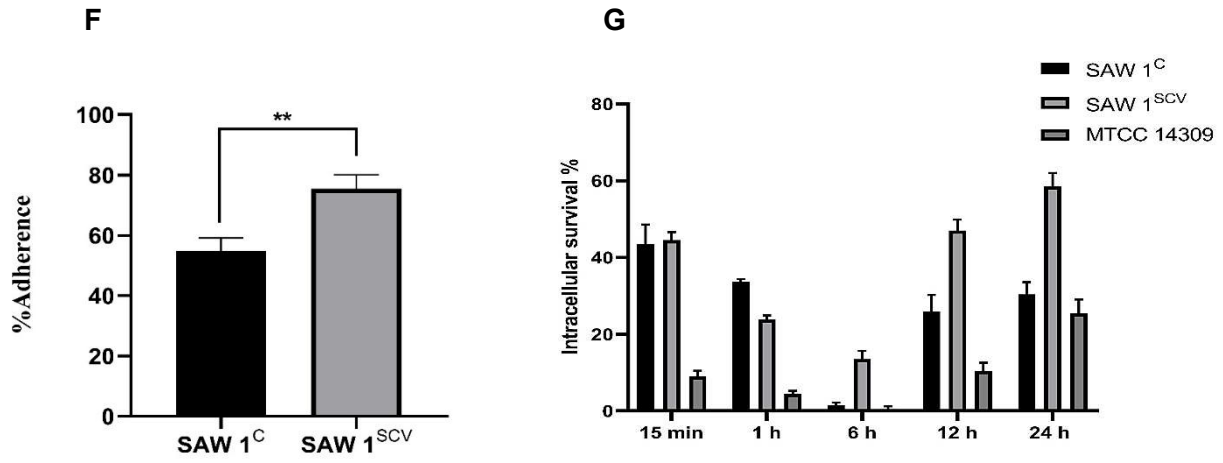


Figure 4: Stability and growth characteristics of SCVs upon prolonged ZnO NP exposure

(A) Schematic representation of experimental evolution to enrich *S. aureus* small colony variants (SCVs) under subinhibitory ZnO nanoparticle (NP) pressure and corresponding media-only control. SAW1 culture was repeatedly exposed to 500 µg/ml ZnO NPs over 14 passages. A single SCV colony was selected at each passage to inoculate the next culture. Serial passaging under ZnO NP pressure led to progressive enrichment and phenotypic stabilization of SCVs, whereas repeated passaging in media alone did not induce SCV formation. (B) Population shift from *S. aureus* SAW1^{C} to small colony variant SAW1^{SCV} over serial passages (P1-P14) under subinhibitory ZnO NP exposure. Bar graph shows the increasing percentage of SCVs with passage number, indicating selection and enrichment of the SCV phenotype. (C) Colony morphology on TSA plates at 36 h shows the typical parental (SAW1^{C}, left) and the stable SCV phenotype (SAW1^{SCV}, right) maintained after removal of ZnO NP pressure at passage 12, indicating heritable stability. (D) Growth kinetics of SAW1^{C} and SAW1^{SCV} in TSB medium over 24 h. SCVs exhibit an extended lag phase and reduced growth rate. (E) Generation time analysis reveals significantly increased doubling time in SAW 1^{SCV} compared to SAW 1^{C} (***$p < 0.001$), consistent with the slow-growing SCV phenotype. Error bars represent standard deviation from biological replicates. (F) Intracellular survival (%) of SAW 1^{C} (parental strain), SAW 1^{SCV} (small colony variant), and the laboratory reference strain, MTCC 14309 was assessed at 15 min, 1 h, 6 h, 12 h, and 24 h post-infection. (G) Adherence of SAW1^{C} and its small colony variant SAW1^{SCV} to human lung epithelial A549 cells was quantified using an adherence assay. SAW1^{SCV} exhibited significantly higher adherence (75.45 %) than SAW1^{C} (54.72 %) with a mean difference ± SEM of 20.73 ± 3.697. Statistical significance was determined by an unpaired two-tailed t-test, $p < 0.01$. Experiments were performed in replicates (n=3).

Emergence of non-canonocal mutations in SCVs enriched by ZnO nanoparticle exposure

To uncover genetic determinants underlying the emergence of small colony variants (SCVs) upon ZnO nanoparticle (NP) exposure, WGS was performed at passage 12 (P12) on two independently isolated SCV colonies from the ZnO NP exposed population and two colonies from the corresponding untreated SAW 1^{C} population.

Genomic DNA was extracted using standardized protocols and subjected to short-read sequencing. Assemblies generated using Shovill and SPAdes were quality-checked using QUAST and CheckM. Species identity was verified using PGAP and TYGS pipelines, confirming both isolates as *S. aureus*, with conserved virulence gene profiles and identical MLST types.

Genome assembly generated 17 contigs for the parental strain (*S. aureus* SAW 1^{C}) and 15 contigs for the SCV isolate (SAW 1^{SCV}), with assembled genome sizes of 2,797,119 bp and 2,778,321 bp, respectively.

Both genomes exhibited comparable GC content (32.73–32.77%) and similar numbers of rRNA, tRNA, and tmRNA genes, although the SCV genome contained a slightly reduced number of predicted coding sequences **(Table 1).** Circular genome maps of the SAW 1^{C} and SAW 1^{SCV} isolates revealed a high degree of overall genomic conservation, with no large-scale chromosomal rearrangements apparent between the two strains **(Figure S5)**. Genome-based phylogenetic analysis revealed that both the SAW1^{C} and the evolved SAW1^{SCV} clustered most closely with *S. aureus* DSM 20231, confirming their taxonomic identity and high genomic relatedness to the *S. aureus* species **(Figure S6)**.

SCV genome carries non-canonical mutations

Crucially, the SCV genome lacked mutations in classical SCV- associated genes such as *hem*B, *men*D, *thy*A, or *rpo*B[37,55], suggesting non-canonical genetic mechanism driving this persistent

phenotype. We identified point mutations in SAW 1^{SCV} genome (**Table 2**), encompassing *mpr*F (N477D), *rps*E (A56V), *gyr*A (S739G), *yqeH* (stop-codon loss) and *com*EB (G25D). Among these, mutations in *mprF*, *gyrA* and *yqeH* likely to have greatest functional significance, whereas mutation in *rpsE* A56V substitution represents a conservative change between nonpolar residues, and the synonymous *narZ* variant does not alter the encoded amino acid and is therefore less likely to have a direct effect on protein function. These mutations implicate cellular processes such as membrane charge modulation (*mpr*F), ribosomal function (*rps*E) and (*yqe*H), DNA supercoiling (*gyr*A), and competence regulation (*com*EB). The *mpr*F gene product is a bifunctional lysyl-phosphatidylglycerol synthetase/flippase that have been reported to modify membrane charge to repel cationic antimicrobial peptides including daptomycin.[56,50] Mutations in *mprF* may contribute to SCV associated persistence and membrane remodeling, promoting survival under cationic Zn^{+2}. The *gyrA* mutation disrupts DNA topology and replication, contributing to reduce growth rates. Although mutations in *gyrA* have not been previously reported as a canonical driver of SCV formation, studies have demonstrated that alterations in DNA superhelicity constitute an important bacterial response to environmental stress.[57] For instance, stress-induced changes in DNA supertwist have been reported in *Bacillus subtilis*, suggesting that modulation of chromosome topology represents a conserved adaptive mechanism for reprogramming cellular physiology under adverse conditions.[59] Although less well characterized, the *comEB* mutation may alter bacterial competence and stress adaptation pathways, consistent with phenotypes observed in triclosan-induced SCVs exhibiting reduced competitive fitness and persistence traits potentially due to the impaired cell division.[58]

Of particular interest was a mutation in the *yqe*H gene, which encodes a ribosome biogenesis GTPase. This mutation resulted in the loss of a premature stop codon, potentially extending the protein to 366 amino acids. Although, *yqe*H is poorly characterized in *S. aureus*, its homologs in *E. coli* and *B. subtilis* are members of the circularly permuted GTPase (cpGTPase) family,

functioning as a checkpoint factor in 30S ribosomal subunit assembly during nutrient limitation or oxidative stress conditions.[38, 59]

In several bacteria, *yqe*H is essential for growth, with its GTPase activity closely linked to ribosomal maturation in response to environmental cues.[38] The observed read-through mutation in our SCV isolates may perturb GTPase function or ribosome interactions, potentially modulating translation efficiency or fidelity characteristics of the SCV phenotype.

Bioinformatic analysis revealed that the YqeH protein of WT *S. aureus* SAW1, comprising 123 amino acids, was predicted to be unstable. However, loss of the stop codon resulted in an extended protein of 366 amino acids, which exhibited improved stability. Specifically, the instability index decreased from 48.73 to 34.82. Interestingly, despite the substantial extension in protein length, the aliphatic index and grand average of hydropathicity (GRAVY) remained largely unchanged, shifting only marginally from 102.11 to 101.64 and from -0.226 to -0.220, respectively, suggesting that the overall physicochemical characteristics of the protein were largely preserved. Further comparative analysis of closely related YqeH proteins indicated that the occurrence of shorter and relatively unstable YqeH variants is not uncommon **(Figure S7).**

Furthermore, integrative proteogenomic analysis identified *yqeH*, a circularly permuted GTPase (cpGTPase) of the Obg family, as a potential contributor of adaptation under the ZnO nanoparticle-induced oxidative stress. In this study, proteomic analysis showed strong up-regulation of obg-like GTPases and proteins associated with the ribosome assembly and translation regulation. This suggests *yqe*H may play a role in bacterial adaptation to oxidative stress by remodeling ribosome-associated processes or translational machinery.

These observations raise intriguing questions regarding the evolutionary and functional significance of premature stop codons within *yqeH* across *S. aureus* strains. Whether stop-loss mediated extension of YqeH enhances protein stability, ribosome biogenesis, or stress adaptation, and whether such variants confer a selective advantage under specific environmental conditions, remains to be investigated experimentally.

Plasmid curing and cell wall remodeling drive β -lactam resistance in ZnO NP-adapted *S. aureus* SCVs.

Most notably, the SAW 1^{SCV} genome lacked a ~19 kb plasmid present in the SAW 1^{C}. This plasmid encoded key components of the *bla* operon, including the β-lactamase gene *blaZ* and its regulatory elements *blaI* and *blaR*. A circular map of the lost plasmid is shown **(Figure S8)**.

Previous studies have suggested that maintenance of plasmids imposes a metabolic burden on bacterial cells, particularly under stressful environmental conditions.[60,61] Consequently, plasmid loss can confer a selective advantage by reducing the energetic costs associated with plasmid replication and gene expression. In one study, researchers have shown that plasmid curing in multidrug-resistant *S. aureus* resulted in the loss of resistance markers and restoration of susceptibility to multiple antibiotics.[62] Crucially, despite losing this $blaZ$-mediated enzymatic resistance mechanism, SAW 1^{SCV} exhibited increased phenotypic resistance to PBP-targeting β-lactam antibiotics. This demonstrates that β-lactam resistance in SAW 1^{SCV} may govern by non-enzymatic chromosomal adaptations rather than plasmid retention. These structural adaptations-characteristic of the metabolically quiescent SCV phenotype likely include cell wall thickening, modified peptidoglycan cross-linking, and regulatory alterations in surface charge (e.g., via *mprF* or cell wall stress networks) that physically restrict antibiotic penetration and PBP accessibility.[56,63] Thus, while serial passaging under nanoparticle stress selected for plasmid shedding to optimize bioenergetic fitness, concurrent envelope remodeling **(Figure 3E).** However, the precise mechanisms driving plasmid instability and the fitness consequences of plasmid loss in ZnO NP-adapted SCVs remain to be explored in greater detail.

Table 1: Summary of whole-genome assembly statistics for parental *S. aureus* WT and ZnO NP-induced enriched small colony variant (SAW 1^{SCV})

Strain	Contig	Genome size (bp)	CDS	rRNA	tRNA	tmRNA	GC%
S.aureus WT	17	2797119	2588	7	58	1	32.73
S.aureus SAW 1^{SCV}	15	2778321	2565	7	58	1	32.77

completedness: 99.51; contamination: 0.08

Table 2: SNPs observed between *S. aureus* WT and *S. aureus* SAW 1^{SCV} (Variants were filtered to retain only those with a QUAL score ≥ 20 and read depth (DP) ≥ 30).

Gene name	Product	Contig	Pos	Ref	Alt	Variant effect
*yqe*H	ribosome biogenesis GTPase YqeH	Contig00001	278462	T	C	Stop codon in wild type lost, protein is 366 amino acid long
*com*EB	ComE operon protein 2	Contig00001	283447	G	A	missense variant; G25D
*mpr*F	bifunctional lysylphosphatidyl	Contig00001	542287	T	C	missense variant; N477D

	glycerol flippase/synthetase					
*gyr*A	DNA gyrase subunit A	Contig00004	45998	T	C	missense variant; S739G
*rps*E	30S ribosomal protein S5	Contig00003	66995	G	A	missense variant; A56V
narZ	nitrate reductase subunit alpha	Contig00003	216793	G	A	synonymous variant
Intergenic	-	Contig00001	228950	CAAAAAA	CAAAAAAA	-
Intergenic	-	Contig00003	316506	C	T	-

563

564 **Conclusion**

565 This study provides insights into a new adaptive strategy by which bacteria originally susceptible
566 to ZnO nanoparticles become tolerant to their toxic effects after repeated long-term subinhibitory
567 concentrations. Subinhibitory exposure to ZnO nanoparticles induces the emergence of a
568 persistent SCV phenotype in *S. aureus*. The resulting SCVs exhibited characteristic features
569 including slow growth, altered colony morphology, and cell-wall remodelling. Integrative genomic
570 and proteomic analyses revealed that this adaptation was associated with non-canonical genetic
571 and regulatory changes involving membrane homeostasis, ribosome-associated processes,

plasmid loss, and DNA topology, suggesting that nanoparticle-induced adaptation arises through mechanisms distinct from those classically associated with SCV formation.

Importantly, adaptation to ZnO NP stress did not result in complete resistance to ZnO NPs or broad-spectrum antibiotic cross-resistance. The evolved SCVs remained susceptible to ZnO NPs and showed altered susceptibility to different antibiotics, including increased resistance to selected β-lactams and increased susceptibility to some other antibiotics. These findings indicate that adaptation to ZnO NP stress may involve physiological trade-offs rather than the development of a generalized resistance phenotype.

These findings have implications for the prolonged use of ZnO NP-containing antimicrobial materials, including wound dressings and medical-device coatings, where sustained exposure could impose selective pressure on bacterial populations. Our results indicate that although ZnO NPs remained susceptible against the evolved SCVs, prolonged exposure can select for a slow-growing and more persistent population with increased β-lactam resistance. Understanding such adaptive responses will therefore be important when assessing the long-term antimicrobial efficacy and evolutionary consequences of ZnO NP-based materials.

This study has a few limitations. The experimental evolution was performed using a single clinical *S. aureus* strain, and genomic analysis was based on two independently isolated SCV colonies. The identified mutations were not functionally validated, and therefore their individual contributions to nanoparticle adaptation cannot yet be fully established. Finally, the ZnO NP concentrations used in this study were selected to impose reproducible subinhibitory selective pressure and may exceed concentrations encountered in some real-world applications. These factors should be considered when extrapolating the findings to other *S. aureus* strains and clinical or environmental settings.

Methods

Bacterial Strain and Culture Conditions

The *Staphylococcus aureus* SAW1 strain used in this study is a clinical strain isolated from a patient at Agartala Government Medical College (AGMC) in Agartala, India. This strain was maintained in Tryptic Soy Broth (TSB) or on Tryptic Soy Agar (TSA) plates at 37°C under aerobic conditions.

Synthesis and characterization of ZnO NPs

Zinc oxide (ZnO) nanoparticles used in this study were synthesized and fully characterized by the Department of Chemistry, Jamia Millia Islamia, New Delhi, India.[17] The nanoparticles were prepared via a mechanical-assisted thermal decomposition at 275 °C. X-ray diffraction (XRD) confirmed a pure hexagonal wurtzite ZnO phase, while scanning and transmission electron microscopy (SEM/TEM) revealed a nanorod morphology with an average length of ~1.5 µm, width of ~80 nm, and an aspect ratio of 18.75.[17]

Stability of ZnO NPs

To assess the stability of synthesized nanoparticles under biological testing conditions, various concentrations of ZnO NPs (ranging from 250 to 750 μg/ml) were added to TSB media. The suspensions were incubated at 37°C for 24 h to simulate growth conditions. Their stability was evaluated by acquiring the UV-Vis absorbance spectra across the wavelength range of 300-700 nm after 24 h of incubation.

Nanoparticle Tracking Analysis

The hydrodynamic size and size distribution of synthesized nanoparticles were measured using a Nanoparticle Tracking Analysis (NTA) system (NanoSight NTA 3.4, Build 3.4.4, Malvern

Panalytical) equipped with a Blue488 laser (488 nm) and an sCMOS camera. Samples were diluted 10-fold (1×10^1) in deionized water and injected into the sample chamber. Video captures were recorded in triplicate ($1{,}498$ frames total at 25.0 FPS) under standardized operating parameters (Camera Level: 10, Slider Shutter: 696, Slider Gain: 55) at a temperature maintained between 26.9 and 27.1°C and sample viscosity of 1.0 cP. Particle tracking and size distribution analysis were conducted using NTA software with a detection threshold of 5 to determine the mean, mode, and particle concentration.

Antibacterial activity

The antibacterial activity of zinc oxide nanoparticles (ZnO NPs) against *S. aureus* strain SAW1 was assessed by treating mid-log phase culture (OD_{600} ~0.4) with varying concentrations of ZnO NPs (50, 100, 250, 500, and 750 µg/ml) in TSB at 37°C under aerobic conditions, as described previously.[5] Growth kinetics were monitored using a BioTek Synergy microplate reader (Agilent Technologies Inc., California, USA), measuring the OD_{600} at regular intervals over a 24 h period. To evaluate bacterial viability, endpoint colony-forming units per milliliter (CFU/ml) were determined through serial dilution and plating on TSA, followed by incubation at 37°C for 24 h.

Intracellular ROS generation assay

Reactive oxygen species (ROS) generation was quantified as described previously[23,24] with slight modifications. Briefly, 1 ml of mid-log phase culture was treated with different concentrations mentioned above for 24 h. Then, the culture was centrifuged at 10,000 rpm for 10 min and the media was discarded. The pellet was washed twice with 1X PBS. Then, 100 µL of 10 µM DCFH-DA was added and incubated for 30 min at 37 °C. After incubation, the pellet was washed three times with 1X PBS and centrifuged again at 10,000 rpm for 10 minutes. The pellet was then resuspended in 1X PBS. Next, 100 µL of the resuspended culture was distributed in the dark

across a 96-well plate, and fluorescence was measured at an excitation wavelength of 485 nm and an emission wavelength of 530 nm.

Proteomic analysis

Mid-log phase cultures of *S. aureus* SAW1 were exposed to ZnO NPs at a concentration of 500 µg/ml for 24 h. Following treatment, bacterial cells were harvested by centrifugation and subsequently washed twice with ice-cold PBS. Total protein was extracted using a standard lysis buffer containing 1% SDS and protease inhibitors, followed by quantification using the BCA assay.

For digestion, 50 ug of protein sample was used for digestion and reduced with 5 mM TCEP and further alkylated with 50 mM iodoacetamide and then digested with Trypsin (1:50, Trypsin/lysate ratio) for 16 h at 37 °C. Digests were cleaned using a C18 silica cartridge to remove the salt and dried using a speed vac. The dried pellet was resuspended in buffer A (2% acetonitrile, 0.1% formic acid). Experiments were performed on an Easy-nlc-1000 system coupled with an Orbitrap Exploris mass spectrometer. 1ug of peptide sample were loaded on *C18 column 15 cm, 3.0µm Acclaim PepMap (Thermo Fisher Scientific)* and separated with a 0-40% gradient of buffer B (80% acetonitrile, 0.1% formic acid*)* at a flow rate of 300 nl/min) and injected for MS analysis. LC gradients were run for 60 minutes. MS1 spectra were acquired in the Orbitrap (Max IT = 25ms, AGQ target = 300%; RF Lens = 70%; R=60K, mass range = 375−1500; Profile data). Dynamic exclusion was employed for 30s excluding all charge states for a given precursor. MS2 spectra were collected for top 12 peptides. MS2 (Max IT= 22ms, R= 15K, AGC target 200%). All samples were processed and RAW files generated were analyzed with Proteome Discoverer (v2.5) against the Proteome *S. aureus* database. For dual Sequest and Amanda search, the precursor and fragment mass tolerances were set at 10 ppm and 0.02 Da, respectively. The protease used to generate peptides, i.e., enzyme specificity was set for trypsin/P (cleavage at the C terminus of

667 “K/R: unless followed by “P”). Carbamidomethyl on cysteine as fixed modification and oxidation
668 of methionine and N-terminal acetylation were considered as variable modifications for database
669 search. Both peptide spectrum match and protein false discovery rate were set to 0.01 FDR.
670
671 **Characterization of SCV**

672 **a. Colony diameter**

673 Colony size measurements were conducted to distinguish between WT and small SCV
674 populations based on their physical dimensions. *S. aureus* SAW1 cultures were treated
675 with 500 µg/ml or 750 µg/ml ZnO nanoparticles for 24 h and plated on TSA. Following
676 incubation at 37 °C, plates were photographed once SCVs had visibly emerged. Using
677 ImageJ software (W. S. Rasband, National Institutes of Health, Bethesda, MD)[64], the
678 diameters of 10 representative colonies from each population (WT and SCV) were
679 measured. Colonies with diameters of one-tenth the median WT colony size were
680 classified as SCVs, in accordance with commonly used operational definitions.
681
682 **b. Transmission Electron Microscopy**

683 Fresh single colonies of untreated *S. aureus* and small colony variants that emerged after
684 48 h of incubation were picked and resuspended in 0.1 M phosphate buffer (pH 7.4). The
685 cells were stained with uranyl acetate and observed using a Hitech transmission electron
686 microscope (TEM). The samples were loaded onto copper grids, contrasted with 1%
687 Phosphotungstic acid, and examined using a TECNAI (HR-TEM) operating at 120 kV. Cell
688 wall thickness was measured in 5 cells of each sample with nearly equatorially cut
689 surfaces by ImageJ (W. S. Rasband, National Institutes of Health, Bethesda, MD).[64]
690
691 **c. SCV Stability Assay**

The stability of SCVs after repeated nanoparticle exposure was checked[50] with slight modifications, by conducting a serial passaging enrichment assay under continuous ZnO NP pressure. *S. aureus* SAW1 cultures were treated with 500 µg/ml ZnO NPs in TSB and incubated at 37 °C with agitation at 550 rpm for 24 h in thermomixer C (Eppendorf). Following treatment, cultures were plated on TSA and incubated at 37 °C until colonies developed. A single small colony displaying was isolated and re-inoculated into fresh TSB supplemented with 500 µg/ml ZnO NPs, followed by incubation for another 24 h under identical conditions. This passaging process was repeated for 14 successive cycles (P1-P14), with a single SCV colony selected at each stage to initiate the next round of nanoparticle exposure. After the 12th passage, ZnO NPs were withdrawn to evaluate the phenotypic stability of the enriched population. Colonies that retained SCV features-including reduced size and loss of pigmentation-in the absence of ZnO NPs were considered phenotypically stabilized.

d. Growth profiling and generation time

Standard disc diffusion assays were performed using the Kirby-Bauer method to compare the antimicrobial susceptibility profiles of WT and SAW1^{SCV} *S. aureus* strains. Overnight cultures of both SAW 1^{C} and SAW 1^{SCV} isolates were diluted in fresh TSB to an initial optical density (OD_{600}) of 0.01. Aliquots of 200 µl were dispensed in triplicate into a 96-well microtiter plate (Costar, flat bottom), and the plates were incubated at 37 °C with continuous orbital shaking.

Real-time OD_{600} measurements were recorded at 20-minute intervals over a 24 h period using a BioTek Synergy microplate reader (Agilent technologies inc, Calfornia, USA). Growth curves were generated by plotting OD_{600} versus time, and generation times were calculated from the exponential phase of each growth curve using standard doubling time

equations. All experiments were performed in three independent biological replicates with technical triplicates per condition.

e. Biofilm formation and SYTO 9 staining

Biofilm formation was assessed using overnight bacterial cultures grown in TSB. The overnight cultures were diluted 1:100 into fresh TSB supplemented with 0.2% (w/v) glucose and 200 µL of the diluted suspension was dispensed into sterile, flat-bottom 96-well polystyrene microtiter plates. The plates were incubated statically at 37°C for 24 h to allow biofilm formation.

Following incubation, the culture supernatant containing planktonic cells was carefully removed, and the biofilms were gently washed three times with sterile 1× PBS. For viable biofilm cell enumeration, the attached biofilms were mechanically disrupted by vigorous pipetting and scraping in 1× PBS to obtain a homogeneous cell suspension. Appropriate serial dilutions were prepared, plated TSA, and incubated at 37°C for 18-24 h. CFU were enumerated, and the results were expressed as CFU/ml.

For fluorescence microscopy, the washed biofilms were stained with 50 µL of 2.5 µM SYTO™ 9 (Invitrogen, Thermo Fisher Scientific) and incubated for 15 min at room temperature in the dark. After staining, excess dye was gently removed, and the biofilms were washed once with sterile 1x PBS to minimize background fluorescence. The stained biofilms were visualized using an EVOS M5000 fluorescence microscope (Thermo Fisher Scientific).

f. Antimicrobial Susceptibility Testing

To evaluate the antimicrobial susceptibility profiles of both the SAW 1^{C} and SAW 1^{SCV}

S. aureus strains, standard disc diffusion assays were performed using the Kirby-Bauer method. Bacterial cultures were grown to mid-logarithmic phase, and the cultures were uniformly spread onto TSA plates. Commercially available antibiotic discs (n = 22; HiMedia, India) were placed on the inoculated plates and incubated at 37 °C for 18-24 h. Zones of inhibition were measured and antibiotics that exhibited differential susceptibility between the two strains were further evaluated using MIC testing. MICs were determined by the broth microdilution method following CLSI protocols.

g. A549 cell adhesion assay

To evaluate bacterial adhesion to host epithelial cells, a standardized adhesion assay was performed using A549 human lung epithelial cells.[65] On Day 1, A549 cells were seeded into 24-well tissue culture plates at a density sufficient to reach ~70% confluence and incubated at 37 °C in a 5% CO_2 humidified atmosphere. Cells were washed with warm phosphate-buffered saline (PBS), detached using 400 µl of trypsin-EDTA, and resuspended in RPMI 1640 medium supplemented with 10% fetal bovine serum (FBS) and 1% antibiotic-antimycotic solution. The suspension was diluted, and 1 ml of the cell suspension was added to each well of a fresh 24-well plate.

On Day 2, the medium was replaced with fresh RPMI 1640 medium containing 10% FBS (antibiotic-free), and cells were incubated overnight to allow attachment and recovery. In parallel, bacterial strains (SAW 1^{C} and SAW 1^{SCV}) were grown overnight in TSB at 37 °C with shaking. On Day 3, bacterial cultures were harvested by centrifugation (10,000 RPM, 10 min), washed once with PBS, and resuspended in cold PBS. The suspension was adjusted to an OD_{600} of 0.20, and 150 µl of this bacterial suspension was diluted into 5 ml of RPMI 1640 with 10% FBS to prepare the inoculum. Confluent A549 monolayers were washed with RPMI 1640 and overlaid with 1 ml of the prepared bacterial suspension.

Plates were briefly centrifuged at 100g for 5 min to facilitate contact and incubated for 1 h at 37 °C in a 5% CO_2 incubator.

To quantify adhered bacteria, original inoculum was serially diluted (10^{-1} to 10^{-4} in 1x PBS) and plated on TSA to determine CFU/ml. After incubation, wells were washed three times with PBS to remove non-adherent bacteria. Adherent cells were released by trypsinization (150 µL trypsin, 3 to5 min), followed by the addition of 400 µL of 0.025% Triton X-100 to lyse epithelial cells and release internalized bacteria. The total lysates were vortexed, serially diluted, and plated on TSA to enumerate adherent and internalized bacteria. After overnight incubation at 37 °C, colonies were counted, and percent adhesion was calculated as: % Adhesion = (Adherent and internalized CFU / Original inoculum CFU) × 100

h. Intracellular persistence assay in THP-1 macrophages

To assess the intracellular survival of *S. aureus* strains, we performed macrophage infection assays using differentiated THP-1 human monocytic cells as described in the previous study. [66,67]

THP-1 cells were seeded into 24 well tissue culture plates and differentiated into macrophages by treating with 100 nM phorbol 12-myristate 13-acetate (PMA) for 72 h. After differentiation, the cells were washed and maintained in fresh RPMI 1640 medium supplemented with 10% fetal bovine serum (FBS) for 24 h prior to infection.

Overnight bacterial cultures of SAW 1^{C}, SAW 1^{SCV} and MTCC 14309 strains were washed twice with 1x PBS and adjusted to an optical density corresponding to a multiplicity of infection (MOI) of 1:200. The THP-1 macrophages were infected with 1 ml of bacterial suspension and incubated at 37 °C with 5% CO_2. After 1 h of infection, non-internalised

extracellular bacteria were removed by washing the wells three times with sterile PBS, and fresh RPMI 1640 medium containing 10% FBS and 100 µg/ml gentamicin was added to eliminate remaining extracellular bacteria. The infected macrophages were then incubated for an additional 24 h.

At designated time points-15 min, 1 h, 6 h, 12 h and 24 h post-infection—macrophages were washed three times with PBS and lysed using 0.025% Triton X-100. The lysates were serially diluted in PBS and plated on TSA to enumerate viable intracellular *S. aureus* as colony-forming units (CFU). In parallel, aliquots of the culture supernatant were also plated to confirm the absence of extracellular bacteria.

Whole Genome Sequencing analysis

Genomic DNA was extracted from both $SAW1^{C}$ and $SAW1^{SCV}$ using a standard phenol-chloroform extraction method. The quality and concentration of the DNA were assessed using a NanoDrop spectrophotometer and agarose gel electrophoresis. High-throughput sequencing was conducted on the Illumina platform, resulting in paired-end reads.

The raw sequencing data obtained from Illumina platform was stored in FASTQ files, which contain sequence information (paired-end reads) along with corresponding quality scores (Q scores).[68] Fastpv0.23.2 was used for quality trimming and FastQC v0.12.1 for quality assessment of Illumina reads.[69] The trimming parameters applied were a Q score ≥ 30 and a minimum read length of 100 at its core along with some pre- and post- assembly steps to improve the overall assembly.[70] This resulted in draft assemblies comprising 41 to 61 contigs across all samples. Contigs shorter than or equal to 500 bases were filtered out and the final assemblies were assessed using QUAST v5.3.0. To further assess genome completeness, CheckM v1.2.3 was used. It provides robust estimates of genome completeness and contamination by using collocated sets of genes that are ubiquitous and single-copy within a phylogenetic lineage. The

taxonomy check of PGAP (Prokaryotic Genome Annotation Pipeline) by NCBI was used to assess the taxonomy of the assembly. This check uses the Average Nucleotide Identity (ANI) tool, which compares the query genome against the type strains in GenBank to verify the correct taxonomic classification of the organism. Each assembly reported an ANI value above 98.9% with query and subject coverages exceeding 92%, leading to a CONFIRMED taxonomic status with HIGH confidence for all samples. These results validate the correct classification of the assemblies as *S. aureus*. The detailed result from the taxonomy check is as follows. The TYGS was used, which employs the Genome-to-Genome Distance Calculator (GGDC) to compare the user's genome against a database of reference type (strain) genomes. Following this comparison, TYGS constructs phylogenetic trees that include both branch support and indicators of tree likeness. The genome assemblies of the samples were uploaded to the TYGS platform. TYGS automatically identified the 10 most closely related type strains for each sample, enabling robust comparative analysis.[71] Species and subspecies assignment was made based on established dDDH thresholds and a clustering algorithm that emphasizes taxonomic conservatism and considers nomenclatural priority. The resulting phylogenetic tree included bootstrap support values, which provide a measure of confidence for each branch, supporting the reliability of the inferred relationships. The assembled genomes were used for annotation using Bakta v1.9.4 installed locally and with its own database.[72] The circular maps of the assembled genome were generated using an annotated GBFF file using the Proksee server.[73] Variant calling was performed using BCFtools v1.21 on the samples. Variants were filtered to retain only those with a QUAL score ≥ 20 and read depth (DP) ≥ 30.[74] To assess the potential impact of the identified variants, SnpEff v5.2f was used to annotate the filtered VCFs obtained from the comparisons. [74]

Statistical analysis

All experiments were carried out in biological replicates unless otherwise noted. The data are expressed as mean ± standard deviation (SD) or mean ± standard error of the mean (SEM). For

statistical analysis, we used GraphPad Prism version 9.0 (GraphPad Software, USA). Comparisons between two groups were made using the unpaired Student's t-test, while comparisons among multiple groups were performed using one-way ANOVA. A p-value of less than 0.05 was deemed statistically significant.

Data Availability

The WGS of *S. aureus* SAW1 used in this study is available in NIH National Center for Biotechnology Information at https://www.ncbi.nlm.nih.gov/biosample/50677180, BioProject accession number: PRJNA1307875.

All other data supporting the findings of this study are presented in the paper and/or the supplementary Material

ASSOCIATED CONTENT

Supplementary Information (PDF): Supplementary Table S1 containing Particle size distribution of ZnO nanoparticles determined by nanoparticle tracking analysis. S2-S3 containing proteomic, transcriptomic, and antibiotic susceptibility data; Supplementary Figures S1-S8 including Stability and size distribution of ZnO nanoparticles, KEGG and GO enrichment analyses, STRING interaction networks, circular genome map, phylogenomic analyses, plasmid loss analysis, and YqeH phylogenetic analysis.

AUTHOR INFORMATION

Corresponding Author

Ashwini Chauhan- Department of Microbiology, B.K. Bachawat block, University of Delhi, South campus, New Delhi-110021, India; ORCID ID: 0000-0002-0555-8244

Email: ashwinichauhan@south.du.ac.in

Authors

Anjali Jaiswal- Department of Microbiology, B.K. Bachawat block, University of Delhi, South campus, New Delhi-110021, India; ORCID ID: 0009-0008-8502-3143

Sambuddha Chakraborty- Department of Microbiology, B.K. Bachawat block, University of Delhi, South campus, New Delhi-110021, India; ORCID ID: 0000-0002-4536-7223

Akshit Malhotra- Department of Microbiology, B.K. Bachawat block, University of Delhi, South campus, New Delhi-110021, India; 0000-0003-1965-1922

Sangita Jana- Department of Microbiology, B.K. Bachawat block, University of Delhi, South campus, New Delhi-110021, India.

Ram Karan- Department of Microbiology, B.K. Bachawat block, University of Delhi, South campus, New Delhi-110021, India; ORCID ID: 0000-0002-0555-8244

Present Addresses

N.A.

Author Contributions

The study was conceptualized and supervised by A.C. All experiments primarily done by A.J. Proteomic experiments and data analysis were performed by A.M., S.C., A.J. The manuscript was written primarily by A.J, with support from A.C, A.M. and S.C. Cell culture experiments were carried out by A.J. with help from S.C. Killing and ROS assay experiments were done by S.J. Review and editing done by R.K. and A.C. All authors have given approval to the final version of the manuscript.

Funding Sources

This research was funded by DST-Nanomission (DST/NM/NB/2018/203) and ICMR (OMI/20/2020-ECD-1).

Notes

The authors declare no competing financial interest.

ACKNOWLEDGMENT

The authors would like to acknowledge Delhi University, South Campus for providing the necessary infrastructure to carry out this research. AC would like to thank ICMR and DST-Nanomission for the funding support. We are grateful to Prof. Manika Khanuja (Centre for Nanoscience & Nanotechnology, Jamia Millia Islamia) for providing the nanoparticles. We also acknowledge Sophisticated Analytical Instrumentation Facility-All India Institute of Medical Science (SAIF-AIIMS, New Delhi) for providing TEM facility. We also acknowledge the Central Research Facility (CRF), Indian Institute of Technology Delhi (IIT Delhi) for providing access to the nanoparticle tracking analysis (NTA) facility.

ABBREVIATIONS

ZnO NPs: Zinc oxide nanoparticles, AgNP: Silver nanoparticle, SCV: Small Colony Varant, TCA: Tricarboxylic Acid cycle, ROS: Reactive Oxygen Species, WT: Wildtype, SAW 1^{C}: Untreated controlled passage in media only during evolution experiment referred as parental strain, SAW 1^{SCV}: ZnO NP enriched SCV during evolution experiment, bla: β-lactamase.

References

1. Salam MA, Al-Amin MY, Salam MT, Pawar JS, Akhter N, Rabaan AA, Alqumber MAA. Antimicrobial Resistance: A Growing Serious Threat for Global Public Health. Healthcare (Basel). 2023 Jul 5;11(13):1946. doi: 10.3390/healthcare11131946. PMID: 37444780; PMCID: PMC10340576.

2. Puri B, Vaishya R, Vaish A. Antimicrobial resistance: Current challenges and future directions. Med J Armed Forces India. 2025 May-Jun;81(3):247-258. doi: 10.1016/j.mjafi.2024.07.006. Epub 2024 Sep 19. PMID: 40463612; PMCID: PMC12127279.

3. Sánchez-López E, Gomes D, Esteruelas G, Bonilla L, Lopez-Machado AL, Galindo R, Cano A, Espina M, Ettcheto M, Camins A, Silva AM, Durazzo A, Santini A, Garcia ML, Souto EB. Metal-Based Nanoparticles as Antimicrobial Agents: An Overview. Nanomaterials (Basel). 2020 Feb 9;10(2):292. doi: 10.3390/nano10020292. PMID: 32050443; PMCID: PMC7075170.

4. Rayyif SMI, Mohammed HB, Curuțiu C, Bîrcă AC, Grumezescu AM, Vasile BȘ, Dițu LM, Lazăr V, Chifiriuc MC, Mihăescu G, Holban AM. ZnO Nanoparticles-Modified Dressings to Inhibit Wound Pathogens. Materials (Basel). 2021 Jun 4;14(11):3084. doi: 10.3390/ma14113084. PMID: 34200053; PMCID: PMC8200248.

5. Malhotra A, Chauhan SR, Rahaman M, Tripathi R, Khanuja M, Chauhan A. Phyto-assisted synthesis of zinc oxide nanoparticles for developing antibiofilm surface coatings on central venous catheters. Front Chem. 2023 Mar 23;11:1138333. doi: 10.3389/fchem.2023.1138333. PMID: 37035110; PMCID: PMC10076889.

6. Jiang J, Pi J, Cai J. The Advancing of Zinc Oxide Nanoparticles for Biomedical Applications. Bioinorg Chem Appl. 2018 Jul 5;2018:1062562. doi: 10.1155/2018/1062562. PMID: 30073019; PMCID: PMC6057429.

7. Zhang, C., Sun, R., & Xia, T. (2020). Adaption/resistance to antimicrobial nanoparticles: Will it be a problem?. *Nano Today*, *34*, 100909.

8. Holder AL, Vejerano EP, Zhou X, Marr LC. Nanomaterial disposal by incineration. Environ Sci Process Impacts. 2013 Sep;15(9):1652-64. doi: 10.1039/c3em00224a. PMID: 23880913.

9. Stabryla LM, Johnston KA, Diemler NA, Cooper VS, Millstone JE, Haig SJ, Gilbertson LM. Role of bacterial motility in differential resistance mechanisms of silver nanoparticles and silver ions. Nat Nanotechnol. 2021 Sep;16(9):996-1003. doi: 10.1038/s41565-021-00929-w. Epub 2021 Jun 21. PMID: 34155383.

10. Panáček A, Kvítek L, Smékalová M, Večeřová R, Kolář M, Röderová M, Dyčka F, Šebela M, Prucek R, Tomanec O, Zbořil R. Bacterial resistance to silver nanoparticles and how to overcome it. Nat Nanotechnol. 2018 Jan;13(1):65-71. doi: 10.1038/s41565-017-0013-y. Epub 2017 Dec 4. PMID: 29203912.

11. McNeilly O, Mann R, Cummins ML, Djordjevic SP, Hamidian M, Gunawan C. Development of Nanoparticle Adaptation Phenomena in Acinetobacter baumannii: Physiological Change and Defense Response. Microbiol Spectr. 2023 Feb 14;11(1):e0285722. doi: 10.1128/spectrum.02857-22. Epub 2023 Jan 10. PMID: 36625664; PMCID: PMC9927149.

12. Zhang R, Carlsson F, Edman M, Hummelgård M, Jonsson BG, Bylund D, Olin H. Escherichia coli Bacteria Develop Adaptive Resistance to Antibacterial ZnO

Nanoparticles. Adv Biosyst. 2018 May;2(5):e1800019. doi: 10.1002/adbi.201800019. Epub 2018 Apr 2. PMID: 33103858.

13. Fang Q, Pan X. A systematic review of antibiotic resistance driven by metal-based nanoparticles: Mechanisms and a call for risk mitigation. Sci Total Environ. 2024 Mar 15;916:170080. doi: 10.1016/j.scitotenv.2024.170080. Epub 2024 Jan 12. PMID: 38220012.

14. Mapar M, Rydzak T, Hommes JW, Surewaard BGJ, Lewis IA. Diverse molecular mechanisms underpinning Staphylococcus aureus small colony variants. Trends Microbiol. 2025 Feb;33(2):223-232. doi: 10.1016/j.tim.2024.09.007. Epub 2024 Oct 10. PMID: 39393939.

15. Loss G, Simões PM, Valour F, Cortês MF, Gonzaga L, Bergot M, Trouillet-Assant S, Josse J, Diot A, Ricci E, Vasconcelos AT, Laurent F. *Staphylococcus aureus* Small Colony Variants (SCVs): News From a Chronic Prosthetic Joint Infection. Front Cell Infect Microbiol. 2019 Oct 22;9:363. doi: 10.3389/fcimb.2019.00363. PMID: 31696062; PMCID: PMC6817495.

16. Sirelkhatim A, Mahmud S, Seeni A, Kaus NHM, Ann LC, Bakhori SKM, Hasan H, Mohamad D. Review on Zinc Oxide Nanoparticles: Antibacterial Activity and Toxicity Mechanism. Nanomicro Lett. 2015;7(3):219-242. doi: 10.1007/s40820-015-0040-x. Epub 2015 Apr 19. PMID: 30464967; PMCID: PMC6223899.

17. Sharma R, Khanuja M, Islam SS, Singhal U, Varma A. Aspect-ratio-dependent photoinduced antimicrobial and photocatalytic organic pollutant degradation efficiency of ZnO nanorods. Research on Chemical Intermediates. 2017 Oct;43(10):5345-64.

18. Hassan A, Al-Salmi FA, Saleh MA, Sabatier JM, Alatawi FA, Alenezi MA, Albalwe FM, Meteq R Albalawi H, Darwish DBE, Sharaf EM. Inhibition Mechanism of Methicillin-Resistant *Staphylococcus aureus* by Zinc Oxide Nanorods via Suppresses Penicillin-Binding Protein 2a. ACS Omega. 2023 Mar 6;8(11):9969-9977. doi: 10.1021/acsomega.2c07142. PMID: 36969461; PMCID: PMC10034842.

19. Balaban NQ, Helaine S, Lewis K, Ackermann M, Aldridge B, Andersson DI, Brynildsen MP, Bumann D, Camilli A, Collins JJ, Dehio C, Fortune S, Ghigo JM, Hardt WD, Harms A, Heinemann M, Hung DT, Jenal U, Levin BR, Michiels J, Storz G, Tan MW, Tenson T, Van Melderen L, Zinkernagel A. Definitions and guidelines for research on antibiotic persistence. Nat Rev Microbiol. 2019 Jul;17(7):441-448. doi: 10.1038/s41579-019-0196-3. Erratum in: Nat Rev Microbiol. 2019 Jul;17(7):460. doi: 10.1038/s41579-019-0207-4. PMID: 30980069; PMCID: PMC7136161.

20. Huemer M, Mairpady Shambat S, Brugger SD, Zinkernagel AS. Antibiotic resistance and persistence-Implications for human health and treatment perspectives. EMBO Rep. 2020 Dec 3;21(12):e51034. doi: 10.15252/embr.202051034. Epub 2020 Dec 8. PMID: 33400359; PMCID: PMC7726816.

21. Singh U, Saifi Z, Kumar M, Reimers A, Krishnananda SD, Adelung R, Baum M. Role of structural specificity of ZnO particles in preserving functionality of proteins in their corona. Sci Rep. 2021 Aug 5;11(1):15945. doi: 10.1038/s41598-021-95540-3. PMID: 34354203; PMCID: PMC8342705.

22. Lee W, Yeop J, Heo J, Yoon YJ, Park SY, Jeong J, Shin YS, Kim JW, An NG, Kim DS, Park J, Kim JY. High colloidal stability ZnO nanoparticles independent on solvent polarity and their application in polymer solar cells. Sci Rep. 2020 Oct 22;10(1):18055. doi: 10.1038/s41598-020-75070-0. PMID: 33093600; PMCID: PMC7582139.

23. Eruslanov E, Kusmartsev S. Identification of ROS using oxidized DCFDA and flow-cytometry. Methods Mol Biol. 2010;594:57-72. doi: 10.1007/978-1-60761-411-1_4. PMID: 20072909.

24. Babayevska N, Przysiecka Ł, Iatsunskyi I, Nowaczyk G, Jarek M, Janiszewska E, Jurga S. ZnO size and shape effect on antibacterial activity and cytotoxicity profile. Sci Rep. 2022 May 17;12(1):8148. doi: 10.1038/s41598-022-12134-3. Erratum in: Sci Rep. 2023 Aug 1;13(1):12465. doi: 10.1038/s41598-023-39615-3. PMID: 35581357; PMCID: PMC9114415.

25. Hao Y, Wang Y, Zhang L, Liu F, Jin Y, Long J, Chen S, Duan G, Yang H. Advances in antibacterial activity of zinc oxide nanoparticles against *Staphylococcus aureus* (Review). Biomed Rep. 2024 Aug 30;21(5):161. doi: 10.3892/br.2024.1849. PMID: 39268408; PMCID: PMC11391181.

26. Batchelder JI, Taylor AJ, Mok WWK. Metabolites augment oxidative stress to sensitize antibiotic-tolerant *Staphylococcus aureus* to fluoroquinolones. mBio. 2024 Dec 11;15(12):e0271424. doi: 10.1128/mbio.02714-24. Epub 2024 Oct 30. Erratum in: mBio. 2025 Mar 12;16(3):e0007325. doi: 10.1128/mbio.00073-25. PMID: 39475229; PMCID: PMC11633220.

27. Rasmussen T, Rasmussen A. Bacterial Mechanosensitive Channels. Subcell Biochem. 2018;87:83-116. doi: 10.1007/978-981-10-7757-9_4. PMID: 29464558.

28. Matsumoto Y, Xu Q, Miyazaki S, Kaito C, Farr CL, Axelrod HL, Chiu HJ, Klock HE, Knuth MW, Miller MD, Elsliger MA, Deacon AM, Godzik A, Lesley SA, Sekimizu K, Wilson IA. Structure of a virulence regulatory factor CvfB reveals a novel winged helix RNA binding module. Structure. 2010 Mar 14;18(4):537-47. doi: 10.1016/j.str.2010.02.007. PMID: 20399190; PMCID: PMC2858061.

29. Ming T, Geng L, Feng Y, Lu C, Zhou J, Li Y, Zhang D, He S, Li Y, Cheong L, Su X. iTRAQ-Based Quantitative Proteomic Profiling of *Staphylococcus aureus* Under Different Osmotic Stress Conditions. Front Microbiol. 2019 May 29;10:1082. doi: 10.3389/fmicb.2019.01082. PMID: 31191466; PMCID: PMC6549500.

30. Ha KP, Edwards AM. DNA Repair in *Staphylococcus aureus*. Microbiol Mol Biol Rev. 2021 Dec 15;85(4):e0009121. doi: 10.1128/MMBR.00091-21. Epub 2021 Sep 15. PMID: 34523959; PMCID: PMC8483670.

31. Singh R, Cheng S, Singh S. Oxidative stress-mediated genotoxic effect of zinc oxide nanoparticles on *Deinococcus radiodurans*. 3 Biotech. 2020 Feb;10(2):66. doi: 10.1007/s13205-020-2054-4. Epub 2020 Jan 24. PMID: 32030335; PMCID: PMC6980014.

32. Krishnamoorthy R, Athinarayanan J, Periyasamy VS, Alshuniaber MA, Alshammari G, Hakeem MJ, Ahmed MA, Alshatwi AA. Antibacterial Mechanisms of Zinc Oxide Nanoparticle against Bacterial Food Pathogens Resistant to Beta-Lactam Antibiotics. Molecules. 2022 Apr 12;27(8):2489. doi: 10.3390/molecules27082489. PMID: 35458685; PMCID: PMC9032754.

33. Jaiswal PB, Jejurikar S, Mondal A, Pushkar B, Mazumdar S. Antibacterial Effects of ZnO Nanodisks: Shape Effect of the Nanostructure on the Lethality in Escherichia coli. Appl Biochem Biotechnol. 2023 May;195(5):3067-3095. doi: 10.1007/s12010-022-04265-0. Epub 2022 Dec 15. PMID: 36520354.

34. Luche S, Eymard-Vernain E, Diemer H, Van Dorsselaer A, Rabilloud T, Lelong C. Zinc oxide induces the stringent response and major reorientations in the central metabolism of Bacillus subtilis. J Proteomics. 2016 Mar 1;135:170-180. doi: 10.1016/j.jprot.2015.07.018. Epub 2015 Jul 26. PMID: 26211718.

35. Vidovic S, Elder J, Medihala P, Lawrence JR, Predicala B, Zhang H, Korber DR. ZnO nanoparticles impose a panmetabolic toxic effect along with strong necrosis, inducing activation of the envelope stress response in Salmonella enterica serovar Enteritidis. Antimicrob Agents Chemother. 2015;59(6):3317-28. doi: 10.1128/AAC.00363-15. Epub 2015 Mar 23. PMID: 25801570; PMCID: PMC4432186.

36. Macbeth EK, Todd Rose F, Cheung CY, Harbison-Price N, De Oliveira DMP, Whyte HG, Walker MJ, Hussein M, Velkov T, Neville SL, McDevitt CA, Monk IR, Ferguson SA, Cook GM. Overcoming methicillin resistance in Staphylococcus aureus via metal ion disruption of bacterial metabolism. NPJ Antimicrob Resist. 2026 Jun 15. doi: 10.1038/s44259-026-00233-4. Epub ahead of print. PMID: 42298145.

37. Proctor RA, Kriegeskorte A, Kahl BC, Becker K, Löffler B, Peters G. Staphylococcus aureus Small Colony Variants (SCVs): a road map for the metabolic pathways involved in persistent infections. Front Cell Infect Microbiol. 2014 Jul 28;4:99. doi: 10.3389/fcimb.2014.00099. PMID: 25120957; PMCID: PMC4112797.

38. Chakraborty A, Halder S, Kishore P, Saha D, Saha S, Sikder K, Basu A. The structure-function analysis of Obg-like GTPase proteins along the evolutionary tree from bacteria to humans. Genes Cells. 2022 Jul;27(7):469-481. doi: 10.1111/gtc.12942. Epub 2022 May 24. PMID: 35610748; PMCID: PMC9545696.

39. Bezrukov F, Prados J, Renzoni A, Panasenko OO. MazF toxin causes alterations in Staphylococcus aureus transcriptome, translatome and proteome that underlie bacterial dormancy. Nucleic Acids Res. 2021 Feb 26;49(4):2085-2101. doi: 10.1093/nar/gkaa1292. PMID: 33544858; PMCID: PMC7913683.

40. Sun F, Zhou L, Zhao BC, Deng X, Cho H, Yi C, Jian X, Song CX, Luan CH, Bae T, Li Z, He C. Targeting MgrA-mediated virulence regulation in Staphylococcus aureus. Chem

Biol. 2011 Aug 26;18(8):1032-41. doi: 10.1016/j.chembiol.2011.05.014. PMID: 21867918; PMCID: PMC3163066.

41. Bradley JM, Svistunenko DA, Wilson MT, Hemmings AM, Moore GR, Le Brun NE. Bacterial iron detoxification at the molecular level. J Biol Chem. 2020 Dec 18;295(51):17602-17623. doi: 10.1074/jbc.REV120.007746. PMID: 33454001; PMCID: PMC7762939.

42. Henriquez T, Wirtz L, Su D, Jung H. Prokaryotic Solute/Sodium Symporters: Versatile Functions and Mechanisms of a Transporter Family. Int J Mol Sci. 2021 Feb 13;22(4):1880. doi: 10.3390/ijms22041880. PMID: 33668649; PMCID: PMC7918813.

43. Nakamura H, Kumita H, Imai K, Iizuka T, Shiro Y. ADP reduces the oxygen-binding affinity of a sensory histidine kinase, FixL: the possibility of an enhanced reciprocating kinase reaction. Proc Natl Acad Sci U S A. 2004 Mar 2;101(9):2742-6. doi: 10.1073/pnas.0305795101. Epub 2004 Feb 17. PMID: 14970341; PMCID: PMC365691.

44. Wessler S, Schneider G, Backert S. Bacterial serine protease HtrA as a promising new target for antimicrobial therapy? Cell Commun Signal. 2017 Jan 10;15(1):4. doi: 10.1186/s12964-017-0162-5. PMID: 28069057; PMCID: PMC5223389.

45. Gaupp R, Ledala N, Somerville GA. Staphylococcal response to oxidative stress. Front Cell Infect Microbiol. 2012 Mar 16;2:33. doi: 10.3389/fcimb.2012.00033. PMID: 22919625; PMCID: PMC3417528.

46. Zhou S, Rao Y, Li J, Huang Q, Rao X. Staphylococcus aureus small-colony variants: Formation, infection, and treatment. Microbiol Res. 2022 Jul;260:127040. doi: 10.1016/j.micres.2022.127040. Epub 2022 Apr 20. PMID: 35468490.

47. Rapacka-Zdonczyk A. Beyond Resistance: Phenotypic Plasticity in Bacterial Responses to Antibiotics, Oxidative Stress and Antimicrobial Photodynamic Inactivation. Molecules. 2026 Feb 6;31(3):567. doi: 10.3390/molecules31030567. PMID: 41683545; PMCID: PMC12899298.

48. Shen JP, Chou CF. Morphological plasticity of bacteria-Open questions. Biomicrofluidics. 2016 Jun 10;10(3):031501. doi: 10.1063/1.4953660. PMID: 27375812; PMCID: PMC4902820.

49. Ye, Zhiyi, Tianchi Chen, Qi Zhang, Weiyi Huang, and Lei He. "Advances in research on small colony variants of Staphylococcus aureus." *The Microbe* 8 (2025): 100444.

50. Weaver AJ, Peters TR, Tripet B, Van Vuren A, Rakesh, Lee RE, Copié V, Teintze M. Exposure of Methicillin-Resistant Staphylococcus aureus to Low Levels of the Antibacterial THAM-3ΦG Generates a Small Colony Drug-Resistant Phenotype. Sci Rep. 2018 Jun 29;8(1):9850. doi: 10.1038/s41598-018-28283-3. PMID: 29959441; PMCID: PMC6026174.

51. Vulin C, Leimer N, Huemer M, Ackermann M, Zinkernagel AS. Prolonged bacterial lag time results in small colony variants that represent a sub-population of persisters. Nat Commun. 2018 Oct 4;9(1):4074. doi: 10.1038/s41467-018-06527-0. PMID: 30287875; PMCID: PMC6172231.

52. Cao S, Huseby DL, Brandis G, Hughes D. Alternative Evolutionary Pathways for Drug-Resistant Small Colony Variant Mutants in *Staphylococcus aureus*. mBio. 2017 Jun 20;8(3):e00358-17. doi: 10.1128/mBio.00358-17. PMID: 28634236; PMCID: PMC5478891.

53. Xia H, Tang Q, Song J, Ye J, Wu H, Zhang H. A yigP mutant strain is a small colony variant of E. coli and shows pleiotropic antibiotic resistance. Can J Microbiol. 2017 Dec;63(12):961-969. doi: 10.1139/cjm-2017-0347. Epub 2017 Sep 15. PMID: 28915357.

54. Tuchscherr L, Heitmann V, Hussain M, Viemann D, Roth J, von Eiff C, Peters G, Becker K, Löffler B. Staphylococcus aureus small-colony variants are adapted phenotypes for intracellular persistence. J Infect Dis. 2010 Oct 1;202(7):1031-40. doi: 10.1086/656047. PMID: 20715929.

55. Dean MA, Olsen RJ, Long SW, Rosato AE, Musser JM. Identification of point mutations in clinical Staphylococcus aureus strains that produce small-colony variants auxotrophic for menadione. Infect Immun. 2014 Apr;82(4):1600-5. doi: 10.1128/IAI.01487-13. Epub 2014 Jan 22. PMID: 24452687; PMCID: PMC3993378..

56. Ernst CM, Staubitz P, Mishra NN, Yang SJ, Hornig G, Kalbacher H, Bayer AS, Kraus D, Peschel A. The bacterial defensin resistance protein MprF consists of separable domains for lipid lysinylation and antimicrobial peptide repulsion. PLoS Pathog. 2009 Nov;5(11):e1000660. doi: 10.1371/journal.ppat.1000660. Epub 2009 Nov 13. PMID: 19915718; PMCID: PMC2774229.

57. Dorman CJ, Dorman MJ. DNA supercoiling is a fundamental regulatory principle in the control of bacterial gene expression. Biophys Rev. 2016 Nov;8(Suppl 1):89-100. doi: 10.1007/s12551-016-0238-2. Epub 2016 Nov 14. PMID: 28510216; PMCID: PMC5418507.

58. Forbes S, Latimer J, Bazaid A, McBain AJ. Altered Competitive Fitness, Antimicrobial Susceptibility, and Cellular Morphology in a Triclosan-Induced Small-Colony Variant of Staphylococcus aureus. Antimicrob Agents Chemother. 2015 Aug;59(8):4809-16. doi: 10.1128/AAC.00352-15. Epub 2015 Jun 1. PMID: 26033734; PMCID: PMC4505237.

59. Uicker WC, Schaefer L, Koenigsknecht M, Britton RA. The essential GTPase YqeH is required for proper ribosome assembly in Bacillus subtilis. J Bacteriol. 2007 Apr;189(7):2926-9. doi: 10.1128/JB.01654-06. Epub 2007 Jan 19. PMID: 17237168; PMCID: PMC1855813.

60. Curtsinger HD, Martínez-Absalón S, Liu Y, Lopatkin AJ. The metabolic burden associated with plasmid acquisition: An assessment of the unrecognized benefits to host cells. Bioessays. 2025 Feb;47(2):e2400164. doi: 10.1002/bies.202400164. Epub 2024 Nov 11. PMID: 39529437; PMCID: PMC12126754.

61. San Millan A, MacLean RC. Fitness Costs of Plasmids: a Limit to Plasmid Transmission. Microbiol Spectr. 2017 Sep;5(5):10.1128/microbiolspec.mtbp-0016-2017. doi: 10.1128/microbiolspec.MTBP-0016-2017. PMID: 28944751; PMCID: PMC11687550.

62. Ahmad AAM, Abdelwahab AMO, Fawzy E, Khamis T, Abdelmoneim M, Abd El-Hamid MI. Novel plasmid curing mediated restoration of antimicrobial sensitivity by Nigella sativa extract against multidrug resistant Staphylococcus aureus. Sci Rep. 2026 Jan 18;16(1):2611. doi: 10.1038/s41598-025-33667-3. PMID: 41549085; PMCID: PMC12820097.

63. Cui L, Ma X, Sato K, Okuma K, Tenover FC, Mamizuka EM, Gemmell CG, Kim MN, Ploy MC, El-Solh N, Ferraz V, Hiramatsu K. Cell wall thickening is a common feature of vancomycin resistance in Staphylococcus aureus. J Clin Microbiol. 2003 Jan;41(1):5-14. doi: 10.1128/JCM.41.1.5-14.2003. PMID: 12517819; PMCID: PMC149586.

64. Cai Z, Chattopadhyay N, Liu WJ, Chan C, Pignol JP, Reilly RM. Optimized digital counting colonies of clonogenic assays using ImageJ software and customized macros: comparison with manual counting. Int J Radiat Biol. 2011 Nov;87(11):1135-46. doi: 10.3109/09553002.2011.622033. PMID: 21913819.

65. Yadav B, Jaiswal A, Kumar D, Karad DD, Joshi PR, Kamble DP, Mercier C, Kharat AS. Sub-minimum inhibitory concentrations in ceftazidime exacerbate the formation of Acinetobacter baumannii biofilms. Microb Pathog. 2025 Feb;199:107229. doi: 10.1016/j.micpath.2024.107229. Epub 2024 Dec 14. PMID: 39675437.

66. Yang J, Ji Y. Investigation of Staphylococcus aureus adhesion and invasion of host cells. Methods Mol Biol. 2014;1085:187-94. doi: 10.1007/978-1-62703-664-1_11. PMID: 24085697.

67. Miller M, Dreisbach A, Otto A, Becher D, Bernhardt J, Hecker M, Peppelenbosch MP, van Dijl JM. Mapping of interactions between human macrophages and Staphylococcus aureus reveals an involvement of MAP kinase signaling in the host defense. J Proteome Res. 2011 Sep 2;10(9):4018-32. doi: 10.1021/pr200224x. Epub 2011 Jul 28. PMID: 21736355.

68. Chen S, Zhou Y, Chen Y, Gu J. fastp: an ultra-fast all-in-one FASTQ preprocessor. Bioinformatics. 2018 Sep 1;34(17):i884-i890. doi: 10.1093/bioinformatics/bty560. PMID: 30423086; PMCID: PMC6129281.

69. Leggett RM, Ramirez-Gonzalez RH, Clavijo BJ, Waite D, Davey RP. Sequencing quality assessment tools to enable data-driven informatics for high throughput genomics. Front Genet. 2013 Dec 17;4:288. doi: 10.3389/fgene.2013.00288. PMID: 24381581; PMCID: PMC3865868.

70. Tizabi D, Bachvaroff T, Hill RT. Comparative analysis of assembly algorithms to optimize biosynthetic gene cluster identification in novel marine actinomycete genomes. Frontiers in Marine Science. 2022 Jul 29;9:914197.

71. Meier-Kolthoff JP, Göker M. TYGS is an automated high-throughput platform for state-of-the-art genome-based taxonomy. Nat Commun. 2019 May 16;10(1):2182. doi: 10.1038/s41467-019-10210-3. PMID: 31097708; PMCID: PMC6522516.

72. Schwengers O, Jelonek L, Dieckmann MA, Beyvers S, Blom J, Goesmann A. Bakta: rapid and standardized annotation of bacterial genomes via alignment-free sequence identification. Microb Genom. 2021 Nov;7(11):000685. doi: 10.1099/mgen.0.000685. PMID: 34739369; PMCID: PMC8743544.

73. Grant JR, Enns E, Marinier E, Mandal A, Herman EK, Chen CY, Graham M, Van Domselaar G, Stothard P. Proksee: in-depth characterization and visualization of bacterial genomes. Nucleic Acids Res. 2023 Jul 5;51(W1):W484-W492. doi: 10.1093/nar/gkad326. PMID: 37140037; PMCID: PMC10320063.

74. Li H. A statistical framework for SNP calling, mutation discovery, association mapping and population genetical parameter estimation from sequencing data. Bioinformatics. 2011 Nov 1;27(21):2987-93. doi: 10.1093/bioinformatics/btr509. Epub 2011 Sep 8. PMID: 21903627; PMCID: PMC3198575.

Supplementary Files

This is a list of supplementary files associated with this preprint. Click to download.

- Anjaliet.alSupplementaryInformation.docx